KU LEUVEN

FACULTEIT WETENSCHAPPEN

Transport of Tb radioisotopes

Determination of A1 and A2 values

Vincent VERELST

Promotor: Prof. T.E. Cocolios
Instituut voor kern- en stralingsfysica
(KU Leuven)

Begeleider: *K. Dockx*
Instituut voor kern- en stralingsfysica
(KU Leuven)

Proefschrift ingediend tot het
behalen van de graad van
Master of Science in Physics

Academiejaar 2018-2019

Aan Jacques Deleuil,

Grootse man, groot voorbeeld en grootvader

Preface

This master's thesis aims to calculate activity limits for Tb isotopes so that they can be transported in a safe, cheap, and efficient manner. Monte Carlo are also performed to find the most consistent way of calculating the activity limits. There are many people to thank for me getting to this point.

First of all, I would like to give thanks to my promotor, Prof. Cocolios. His insights and ever inspiring passion for science formed a huge contribution to this work. Next, thank you to my supervisor Kristof Dockx for always finding time in your busy schedule to guide me through this project. Thank you to my office colleagues Greg and Simon for helping me in all my struggles. Also many thanks to Aglaia and Mairi for letting me know I was not alone.

Verder wil ik ook mijn familie bedanken voor alle steun gedurende mijn studententijd. Papa, bedankt voor alle levenswijsheden. Natalie, bedankt om veel van mijn geschreven werken, inclusief deze thesis, vrij van grammiticale fouten te houden. Bij deze ook een speciale vermelding voor mijn sponsor; mama, dankuwel voor alles in de afgelopen 23 jaren!

Ook wil ik alle vrienden die ik al had en gemaakt heb gedurende deze jaren bedanken. Aan al mijn vrienden van de volleybal, dankuwel. Bedankt aan al mijn kotgenoten van de Brabançonnestraat 51 om de tijden in dat gebouw onvergetelijk te maken. In het bijzonder aan Nicolas voor de verjaardagsgeschenken en nog veel meer. Verder bedankt, Matthias, de kleine dagen waren me altijd een genoegen! Ten slotte wil ik ook Birte bedanken voor al haar steun gedurende deze jaren.

Scientific summary

Nuclear medicine is a scientific branch that makes use of radioactive nuclei to diagnose and treat certain diseases. A very interesting chemical element for this purpose is terbium. This element has four different isotopes that can be applied in nuclear medicine. ^{149}Tb and ^{161}Tb can be used in the treatment of diseases using α-therapy and β^-- and Auger therapy, respectively. ^{152}Tb and ^{155}Tb have applications in the Positron Emission Tomography (PET) and Singe Photon Emission Computed Tomography (SPECT) imaging techniques, respectively. Since the four isotopes are chemically similar, they can all bind to the same molecule that is used as a tracer. This makes terbium extremely useful in the branch of nuclear medicine that combines therapy and diagnostics: theranostics.

For the transport of radiopharmaceuticals, so-called A_1 and A_2 values are determined for each radioisotope. These are the activity limits for the isotope to be transported in a type A package as a sealed source or open source, respectively. If the limits are exceeded, the isotope must be transported in a larger and more expensive type B package. The A_1 and A_2 values of ^{152}Tb and ^{155}Tb have not been determined yet, so that these isotopes are subject to very conservative limits.

Right now, the expected activity at which ^{152}Tb is expected to be produced in the future, exceeds its A_2 value. To this end, the Belgian and the international regulation on transport of radioisotopes are investigated. The International Atomic Energy Agency (IAEA) provides regulations on the determination of A_1 and A_2 values using the so-called Q system. This system is used to calculate the activity limits for all four Tb isotopes. For every isotope five Q values, labeled Q_A through Q_E, have to be determined. IAEA defines each Q value and gives the appropriate formulas that need to be used for their calculation. However, it is not specified which source material or interpolation methods for tabulated values needs to be used. A comparison of the values calculated in this work with values calculated by a third-party software, shows that there are indeed some numerical differences between the two calculation methods. After the rounding of the values, the calculated A_1 and A_2 values do agree, except for ^{155}Tb, where they differ slightly.

To overcome this inconvenience, another methodology to calculate Q values is investigated in the last part of this work. Instead of using tabulated values from old experiments, Monte Carlo simulations are performed using the FLUKA software package. There seems to be some discrepancy between the values calculated the numerical way and the values calculated with FLUKA. However, when comparing the Monte Carlo results from this work with literature values that were also obtained using a Monte Carlo method, it seems that this method leads to more consistent results.

Vulgariserende samenvatting

Een atoomkern is opgebouwd uit twee verschillende deeltjes: positief geladen protonen en ongeladen neutronen. Afhankelijk van de verhouding tussen het aantal protonen en neutronen zal de kern stabiel of instabiel zijn. Een instabiele kern zal na verloop van tijd vervallen. Hierbij komen energetische deeltjes, genaamd ioniserende straling, vrij. Dit proces is gekend als radioactiviteit.

Sinds zijn ontdekking, zijn er vele toepassingen van radioactiviteit ontdekt. Een belangrijke daarvan is het gebruik van radioactieve kernen in de nucleaire geneeskunde. Een radioactief element kan aan een bepaald molecule gebonden worden om vervolgens naar een specifieke plaats in het menselijk lichaam gestuurd te worden. Hier kan de straling, uitgezonden door de radioactieve kern, bijdragen aan de diagnose of behandeling van bepaalde ziektes en tumoren. Recente technieken hebben het mogelijk maakt om de diagnose en behandeling te combineren, om zo de straling waaraan de patiënt wordt blootgesteld te minimaliseren.

Een chemisch element dat zeer interessant is voor deze toepassing, is terbium. Dit element heeft maar liefst vier isotopen die toepasbaar zijn in de diagnose en behandeling van tumoren. Doordat deze isotopen dezelfde chemische structuur bevatten, kunnen ze in principe allemaal aan eenzelfde molecule gebonden worden, om zo naar de juiste plaats in het lichaam geleid te worden.

Deze terbium isotopen komen niet voor in de natuur. Ze worden eerst artificieel geproduceerd om vervolgens naar ziekenhuizen gebracht te worden. Aan het transport van radioactief materiaal zijn echter extra regels verbonden. Deze regels zijn opgesteld door het International Atomic Energy Agency (IAEA); een instelling van de Verenigde Naties. In het eerste deel van dit werk worden deze regels verder uitgelegd.

Het soort colli waarin een isotoop vervoerd mag worden, hangt af van zijn activiteit. Dit laatste kan geïnterpreteerd worden als het aantal ioniserende deeltjes dat een kern uitzendt per seconde. Als de activiteit van een isotoop beneden een bepaalde limiet ligt, mag deze in een zogenaamde type A colli vervoerd worden. Worden deze limieten overschreden, moet het isotoop in een veel duurder en groter type B colli vervoerd worden. Deze limieten moeten voor elk isotoop apart bepaald worden met het zogenaamde Q systeem, dat werd uitgewerkt door het IAEA. Als voor een isotoop de grenzen voor type A nog niet bepaald zijn, is het onderhevig aan zeer conservatieve limieten. Dit is ook het geval voor de isotopen van terbium, waardoor deze met hun huidige geproduceerde activiteit in een type B colli moeten vervoerd worden.

In dit werk wordt het Q systeem dan ook bestudeerd, teneinde activiteitlimieten te bepalen voor de terbium isotopen, zodat deze in type A colli mogen vervoerd worden. Om dit te doen, moet gekeken worden naar de radioactieve dosis die wordt opgenomen door een transportmedewerker, in geval dat de verpakking beschadigd geraakt. De dosis geeft een maat van schade aan die de werknemer oploopt en mag dan ook bepaalde waardes niet overschrijden. In eerste instantie, wordt in dit werk deze opgelopen dosis bepaald met numerieke methodes, zoals deze beschreven worden in rapporten van het IAEA. De richtlijnen voor de numerieke methodes zijn echter vaak voor interpretatie vatbaar en zijn soms gebaseerd op willekeurige aannames. Door deze reden, worden in het laatste deel van dit werk de opgelopen dosissen bepaald met behulp van simulaties. Deze maken gebruik van de zogenaamde Monte Carlo methode. Dit maakt het mogelijk om zeer accuraat de interactie van energieke deeltjes met de omgeving te simuleren, om zo de dosis te bepalen.

List of Abbreviations

ARBIS	Algemeen Reglement op de Bescherming van de bevolking, van de werknemers en van het leefmilieu tegen het gevaar van Ioniserende Stralingen	p.26
BEIR	Committee on the Biological Effects of lonizing Radiation	p.24
BR2	Belgian Reactor 2	p.1
CERN	Conseil Européen pour la Recherche Nucléaire	p.1
DNA	DeoxyriboNucleic Acid	p.16
Euratom	European Atomic Energy Community	p.24
FANC	Federaal Agentschap voor Nucleaire Controle	p.24
IAEA	International Atomic Energy Agency	p.24
ICRP	International Commission on Radiological Protection	p.18
ICRU	International Commission on Radiation Units and Measurements	p.18
ISOLDE	Isotope Separation OnLine DEvice	p.1
Kerma	Kinetic Energy Released Per Unit Mass	p.19
LET	Linear Energy Transfer	p.19
LNT	Linear No-Threshold Model	p.18
MEDICIS	MEDical Isotopes Collected from ISOLDE	p.1
NORM	Naturally Occurring Radioactive Material	p.28
PET	Positron Emission Tomography	p.21
SCK•CEN	StudieCentrum voor Kernenergie	p.1
SEAL	System for calculating Exemption and A_1 and A_2 Limits	p.44

SPECT	Single Photon Emission Computed Tomography	p.22
UNSCEAR	United Nations Scientific Committee on the Effects of Atomic Radiation	p.24

Contents

1 | Introduction

Ever since the discovery of radioactivity, many applications of this phenomenon have been investigated. While the dangers of ionising radiation became clear very soon, other - beneficial - applications were also discovered. In 1932 Nobel laureate Ernest Lawrence patented his invention of the cyclotron. [1] This particle accelerator made it possible to artificially produce a variety of radionuclides. In 1936 John Lawrence used ^{32}P, a radioisotope produced with his brother's invention - to treat leukaemia. This moment is often considered to mark the birth of the interdisciplinary domain called nuclear medicine. [2] Since then, a lot of research has been dedicated to the use of radioisotopes in both the treatment, as well as the diagnostics of diseases such as cancer.

At the Isotope Separation OnLine DEvice (ISOLDE) facility at the *Conseil Européen pour la Recherche Nucléaire (CERN)*[1] a new facility called MEDical Isotopes Collected from ISOLDE (MEDICIS) has been dedicated to the production of radioisotopes for nuclear medicine since 2017. It will do so by recovering the proton beam used at ISOLDE before it reaches the beam dump. [3] One interesting element produced at CERN-MEDICIS is terbium. With four isotopes - ^{149}Tb, ^{152}Tb, ^{155}Tb and ^{161}Tb - that have use in either the treatment or diagnostics of cancer, it is sometimes called the swiss-army knife for nuclear medicine. The details of the use of the Tb isotopes are explained in chapter 2.

While ^{149}Tb, ^{152}Tb and ^{155}Tb are being produced at CERN-MEDICIS, ^{161}Tb is being produced at the Belgian Reactor 2 (BR2) at the *StudieCentrum voor Kernenergie (SCK•CEN)*.[2] This research reactor, which is active since 1962, works on uranium and produces 20 % to 25 % of all artificial radioisotopes in the world. [4]
One particular challenge after the production of radioisotopes is their transport to other institutions such as hospitals. The most important factor in the transport of radioactive materials is the packaging. Every known radioisotope has its own activity limits for transport, called A_1 and A_2 values. If the activity of the transported isotope is below the limit, it is allowed to be transported in a so-called type A package. When the limits are exceeded, however, the isotopes have to be transported in the much more expensive and larger type B packages. The regulation on nuclear transport is further elaborated in chapter 3.

While for ^{149}Tb and ^{161}Tb the A_1 and A_2 values have already been determined, the same is not true for ^{152}Tb and ^{155}Tb. This means the latter are subject to very conservative limits. The general rules on how to determine the activity limits are also explained in

[1] European Organisation for Nuclear Research.
[2] Study centre for nuclear energy.

chapter 3. After that, chapter 4 discusses the exact methodologies used to calculate the activity limits for the Tb isotopes. The calculated values are subsequently compared to the previously calculated limits for ^{149}Tb and ^{161}Tb.

Since the previously discussed methodologies to calculate activity limits are based mostly on the interpolation of tabulated values, another method was investigated. In chapter 5 a Monte Carlo method using the FLUKA tool is discussed. The activity limits are calculated using FLUKA and, subsequently, compared to values that have already been determined earlier using the same FLUKA software. Doing this, it can be investigated which of the two methods leads to the most consistent and reliable results. Once the most consistent method has been found, it will be used to determine the activity limits for ^{152}Tb and ^{155}Tb.

2 | Theoretical Background

Neutrons and protons are the building blocks of the nucleus. The amount and ratio in which both occur will determine whether a nucleus is stable or not. An unstable nucleus will eventually decay and emit ionising radiation. This chapter will deal with the properties of this radiation, such as its origin, its different forms and its interaction with the environment. Furthermore, the framework of radiation protection will be explained by looking at the biological effects of ionising radiation. Lastly, the role of ionising radiation in the medical world will be considered, with a focus on Tb isotopes.

2.1 Fundamentals of Radioactivity

2.1.1 Radioactive decay

The decay of an unstable nucleus is a random process, i.e. at a given time the nucleus will have a certain probability of decaying. Furthermore, it should be noted that this probability will not change in time. Assume an ensemble of unstable, identical nuclei, with $N(t)$ denoting the amount of nuclei in the ensemble at a given time t. The change of this amount over time is then given by the following differential equation:

$$\frac{dN(t)}{dt} = -\lambda N(t). \tag{2.1}$$

Where λ is the - always positive - decay constant of a certain isotope. It is usually expressed in s^{-1}. If at $t = 0$ there are $N(0)$ isotopes, the solution of (2.1) is

$$N(t) = N(0)\exp(-\lambda t). \tag{2.2}$$

The half-life $t_{1/2}$ of a nucleus is defined as $N(t_{1/2}) = \frac{N(0)}{2}$; the time after which half of the original amount in the ensemble remain, so that from (2.2)

$$t_{1/2} = \frac{\ln(2)}{\lambda} \tag{2.3}$$

Clearly the half-life does not depend on the initial amount of nuclei in the ensemble and is therefore an inherent property for every isotope. Lastly, the activity $A(t)$ of an ensemble is defined as its decay rate so that $A(t) \equiv \lambda N(t)$. Activity is expressed in decays per second: becquerel (Bq). It also follows the exponential decay law. [5]

$$A(t) = A(0)\exp(\lambda t). \tag{2.4}$$

A nucleus can decay in different ways, as will be discussed in the next section. Radioactive decay can be considered as a nuclear reaction starting from a so-called parent nucleus and ending in a so-called daughter nucleus and some decay particles. The particles emitted in radioactive decay will have specific energies, expressed in electronvolt (eV). The sum of the masses of all nucleons is always larger than the mass of the atomic nucleus itself. This is because some mass is converted into energy that keeps the nucleus together by the famous relation $E = mc^2$. Denote with ${}^A_Z X$ an isotope with mass number A and atomic number Z. The isotope therefore contains Z protons and $A - Z$ neutrons. The nuclear binding energy of ${}^A_Z X$ is then defined as

$$B = (Zm_p + (A - Z)m_n - m_X - Zm_e)c^2, \tag{2.5}$$

where m_p, m_n, m_X and m_e stand for the proton, neutron, parent atom and electron mass [MeV / c^2] respectively. The binding energy can be interpreted as the minimum energy required to break up a nucleus. In figure 2.1 a graph can be found that shows the binding energy per nucleon for different isotopes. A striking feature of this graph is the high binding energy of ^{4}He compared to its neighbours.

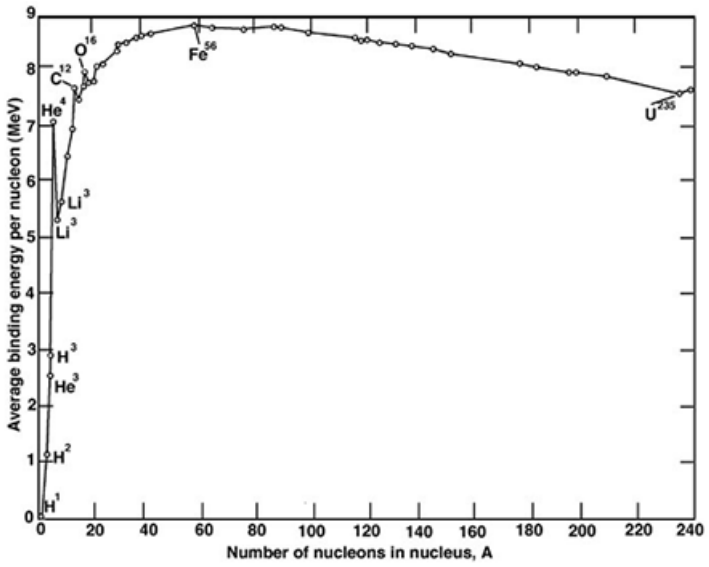

Figure 2.1: Nuclear binding energy graph. [6]

The stability of a nucleus is determined by the interplay of the short range attractive nuclear force (~ 1 fm)[1] between all nucleons and a repulsive Coulomb force between the protons. [7]. Figure 2.2 represents all known isotopes. The isotopes indicated in black are the stable ones. All the other colours represent unstable isotopes that decay through various mechanisms discussed in the next section.

[1] 1 fm = 10^{-15} m.

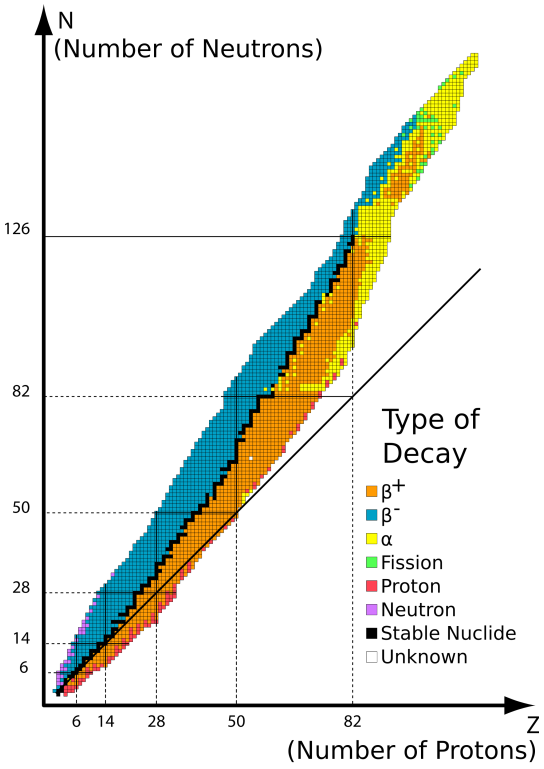

Figure 2.2: Nuclear chart of isotopes. [8]

2.1.2 Types of radiation

Alpha decay

As seen in figure 2.2, alpha decay - represented by the yellow isotopes - typically occurs only for the heavier elements. The reason is that only the heaviest isotopes have a nuclear radius that is large enough in order for the Coulomb repulsion to be stronger than the short range, attractive nuclear force. An alpha decay process can be expressed by the following reaction equation:

$$ {}^{A}_{Z}X \rightarrow {}^{A-4}_{Z-2}X' + {}^{4}_{2}\mathrm{He}. \tag{2.6} $$

${}^{4}_{2}\mathrm{He}$ is also called an α-particle.

In 1928 Gurney and Condon [9] published a theory to explain the mechanics of alpha decay. Because of its relatively high binding energy (see figure 2.1), the alpha particle can be considered a particle moving in a potential well, originated from the daughter nucleus. Alpha decay can then be understood as the tunnelling of the alpha particle out of the potential well. [9] The Q value [MeV] of a nuclear reaction is defined as the mass difference between the parent nucleus and the decay products. For alpha decay the Q value is then given by

$$ Q = (m_X - m_{X'} - m_\alpha)c^2, \tag{2.7} $$

where m_i [MeV / c^2] stands for the mass of particle i. Alpha decay is only energetically and spontaneously possible if $Q > 0$, the energy released by the reaction is then converted into kinetic energy of the daughter nucleus ($T_{X'}$) and α-particle (T_α). Non-relativistic

kinematic calculations lead to

$$T_\alpha = \left(1 - \frac{4}{A}\right) Q. \tag{2.8}$$

Typical values for T_α vary from 4 MeV to 6 MeV. The energy of the alpha particle is specific for the alpha decay itself. [10]

Beta decay

Beta decay is a term generally describing three different processes. Isotopes with an excess amount of neutrons will decay through β^--decay. In this process a neutron will convert in a proton, with the simultaneous release of an electron (e^-) and an electron antineutrino ($\bar{\nu}_e$), through the weak interaction. So that the reaction is given by

$${}^A_Z X \rightarrow {}^A_{Z+1} X' + e^- + \bar{\nu}_e. \tag{2.9}$$

The emitted electron is also called a β^--particle. Ignoring the atomic electron binding energies and the very low neutrino masses [11] the Q-value for this reaction is

$$Q_{\beta^-} = (m({}^A_Z X) - m({}^A_{Z+1} X'))c^2, \tag{2.10}$$

So that β^--decay is energetically possible as long as the daughter mass is lower than the parent mass.
A nucleus with an excess amount of protons will decay through β^+-decay, in which the opposite will happen. A proton will convert in a neutron, while simultaneously releasing a positron (e^+) and an electron neutrino (ν_e).

$${}^A_Z X \rightarrow {}^A_{Z-1} X' + e^+ + \nu_e. \tag{2.11}$$

The positron is also called the β^+ particle. The Q-value for β^+ decay is

$$Q_{\beta^+} = (m({}^A_Z X) - m({}^A_{Z+1} X') - 2m_e)c^2, \tag{2.12}$$

so that it is only energetically possible if the parent mass exceeds the daughter mass by at least two electron masses (~ 1.022 MeV/c^2 [12]).
If a nucleus has an excess amount of protons, there is another way to convert the proton into a neutron: electron capture. In this process an orbital electron of the atom will combine with a proton in the nucleus to form a neutron, while also emitting an electron neutrino. [13]

$${}^A_Z X + e^- \rightarrow {}^A_{Z-1} X' + \nu_e. \tag{2.13}$$

In contrast to alpha decay, the energy spectrum of beta particles is a continuous spectrum varying from zero to the so-called endpoint energy, which is defined as the Q-value of the associated decay (eq. 2.10 and eq. 2.12). The reason for this is purely kinematic: conservation of energy and momentum will not lead to a unique solution for a three-body problem. In other words, the released energy is shared between the beta particle and the (anti)neutrino. [14]

Gamma decay

The previously discussed nuclear decays, as well as other nuclear reactions often leave the daughter nucleus in an excited state. When a nucleus is in an excited state it will de-excite to a lower energy state. In this process a photon is emitted with an energy equal to the energy difference between the two states. This decay happens with a half-life that is typically lower than 10^{-9} s. In figure 2.3 the decay scheme for ^{22}Na can be found. It will decay through β^+ and electron capture decay to ^{22}Ne, leaving it in the 2^+ first excited state for 99.9% of the time. This short-lived excited state ($T_{1/2}$ = 3.7 ps) will de-excite to the ground state, emitting a photon with an energy of 1274 keV.

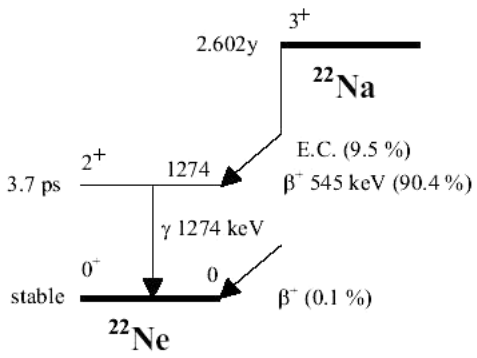

Figure 2.3: Decay scheme of ^{22}Na. [15]

Gamma-ray photons are usually observed with an energy above $\sim$ 124 keV. [16] There exist, however, other mechanisms that also emit photons, not always in the gamma ray spectrum.
After β^+ decay the emitted positron will encounter its anti-particle: the electron. It will subsequently undergo positron-electron annihilation, creating two anti-parallel photons with an energy of 511 keV - the rest mass of an electron - as a result. [17]
Much like in the nuclear case, the orbital electrons of an atom can be in an excited state. The excited electron will de-excite to a lower energy state, emitting a photon with an energy equal to the energy difference between the two states. An atomic photon emitted in this way is called an X-ray. [18]
Lastly, X-rays can also be emitted when a fast electron travels through a medium and is decelerated. In that case bremsstrahlung will be emitted in the process. [19]

Other mechanisms

When a nucleus has an excess of one nucleon over the other, it will normally undergo β decay. If, however, the excess is large enough, the nucleon will essentially become unbound and as a consequence it will be emitted. The limit at which this happens is called the proton/neutron drip-line. [20]
The energy released during the de-excitation of a nucleus can also be transferred to one of the orbital electrons, such that the electron is emitted. This process is called internal conversion. The energy of the electron will be equal to the energy released in the de-excitation minus its own binding energy. [21] The atomic analogue of internal conversion exists as well. When an atom de-excites, that energy can also be transferred to an orbital electron so that it is emitted. Those electrons are called Auger electrons. [22] Finally, very

large nuclei may undergo spontaneous nuclear fission governed by the coulomb interaction. The parent nucleus will split into two smaller daughter nuclei, along with the emission of neutrons. [23]

2.2 Interaction of Radiation with Matter

Ionising radiation is defined as radiation with an energy high enough to ionise the atoms in the environment through which it travels, also called absorber atoms. Figure 2.4 shows the first ionisation energy for the first 20 atoms in the periodic table. This is the energy required to ionise that atom from the ground state to the first ionic state. The local maxima represent the noble gasses, while the local minima belong to the alkali metals. [24]

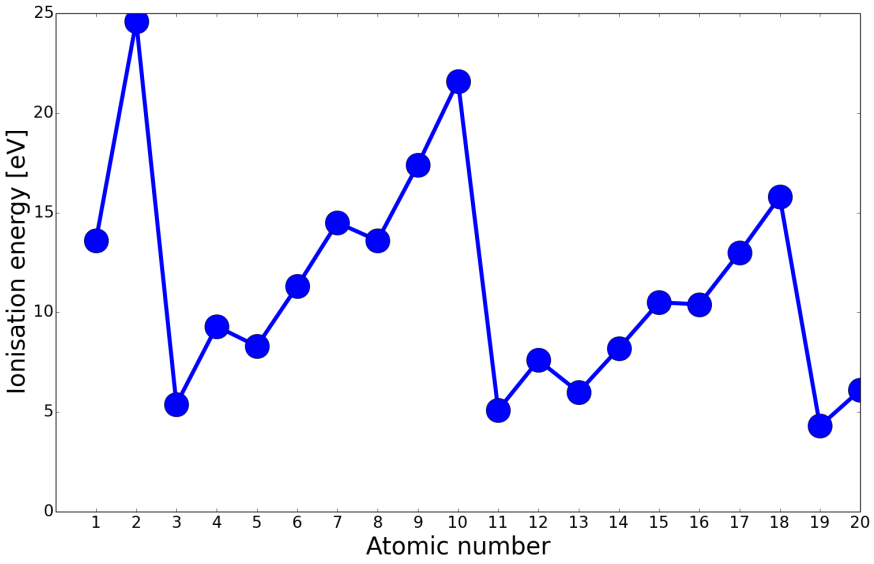

Figure 2.4: First ionisation energies for the first 20 atoms.

Beside its energy, the very nature of a particle will be the deciding factor in how it will interact with matter. In general, there is a distinction between charged radiation and neutral radiation. Both will be discussed separately. [25]

2.2.1 Charged particles

This category includes alpha particles, protons, and all beta particles. All charged particles will interact through the coulomb force with matter; the charged ionising particle will interact with the negative orbital electrons that are omnipresent. Through the interactions, the absorber atoms will either be excited or even ionised. With each interaction the ionising particle will lose energy equal to the excitation or ionisation energy. This is called absorption. These small discrete energy losses can be approximated in a continuous parameter: the stopping power S. The stopping power is defined as the differential energy

loss dE along a differential path dx, travelled by the charged ionising particle

$$S \equiv -\frac{dE}{dx}. \tag{2.14}$$

Since the energy will decrease along the path, the minus sign ensures that S is positive. The stopping power will still be very different for heavy and light particles. The deterministic nature of definition (2.14) conceals the fact that the energy loss of an ionising particle is a stochastic process. The interactions with the absorber atoms happen randomly and, as a consequence, identical ionising particles with the same initial energy will not always have the same energy after travelling the same distance through the same medium. This is known as energy straggling. Figure 2.5 shows an example of the distribution of energies of identical particles with the same initial energy at different points in space as they travel through the medium.

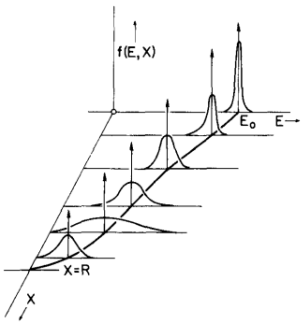

Figure 2.5: Graphical representation of energy straggling. [26]

Another useful quantity to define is the particle range. In theory, this is defined as the distance necessary to completely stop the ionising particle. However, because of energy straggling, this distance will not be the same even for identical, monoenergetic particles. For this reason, workable definitions of the range are constructed for different particles; this will be discussed further on.

Charged heavy particles

For heavy, positively charged particles (heavy ions, protons, alpha particles) with charge ze and velocity v, travelling in a medium with atomic density N and atomic number Z, Bethe found a relativistic formula for the stopping power S [MeV cm^{-1}] in 1932 [27]:

$$S = \frac{4\pi e^4 z^2}{m_e v^2} NZ \left[\ln\left(\frac{2m_e v^2}{I}\right) - \ln\left(1 - \frac{v^2}{c^2}\right) - \frac{v^2}{c^2} \right]. \tag{2.15}$$

I stands for the mean excitation potential of the absorber atoms. In 1933 Bloch showed that $I \simeq 10Z$ [eV]. [28] In the non-relativistic limit ($v \ll c$) the last two terms in the square brackets will vanish. The most important takeaways are the facts that 1) the stopping power is proportional to the electron density NZ, 2) the stopping power is also proportional to z^2 and 3) at low energies, it will decrease approximately as $1/v^2$. This last property is explained by the ionising particle spending longer times in the vicinity of the absorber atoms at lower velocities, thus increasing the energy transfer.

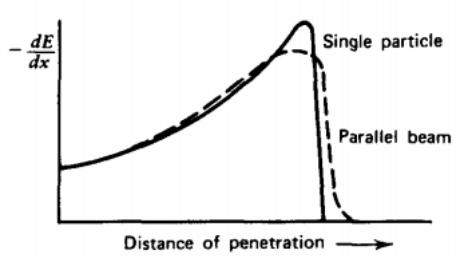

Figure 2.6: Typical bragg curve for α-particles. [25]

In figure 2.6 (full line) the typical stopping power in function of the distance of penetration for a heavy, ionising particle can be seen. This is called a Bragg curve, named after its discoverer W.H. Bragg. [29] The initial increasing behaviour can be explained from the non-relativistic version of equation (2.15). The stopping power will increase with $1/E$ and the energy decreases with travelled distance. After the ionising particle has lost enough energy it will pick up an orbital electron, reducing its charge and thus reducing the stopping power. When the charged particle has picked up enough electrons to be electrically neutral, the stopping power will drop to zero. This phenomenon is also seen in the peak observed in the end of the graph; this is called a Bragg peak. The energy at which electron pickup occurs will be higher for the higher charged particles. The dotted line of the graph in figure 2.6 is a manifestation of energy straggling. The electron pickup will occur at different times for two identical particles, so that the combined Bragg peak is widened.

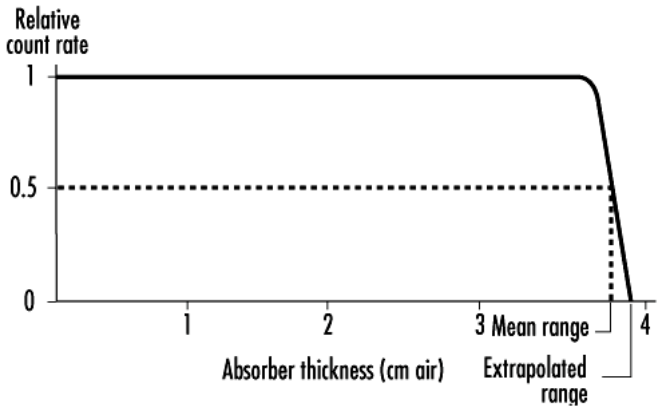

Figure 2.7: Typical range curve for α-particles in air. [30]

With this knowledge the range of heavy charged particles can be defined experimentally. Consider a source emitting ionised particles with an intensity I_0, the particles then pass a certain medium with thickness t. At the end of that medium a detector is placed that counts the incoming particles $I(t)$. Figure 2.7 shows the typical plot of $I(t)/I_0$ versus the thickness t in the ideal case. Up until a certain thickness none of the ionising particles are stopped. Beyond that, suddenly all ionising particles are stopped in a very short range of thicknesses, thus reducing the initial flux of the ionising beam. This process is called attenuation. The reasons that not all particles are stopped at exactly the same thickness is again found in the stochastic nature of the interactions. From this curve two definitions of the range are determined. The mean range is defined as the thickness that

causes exactly half off all particles being stopped. The extrapolated range is the value obtained by linearly extrapolating the end part of the curve to zero. Both definitions of the range are indicated in figure 2.7. As can be seen from the Bethe formula (eq. (2.15)) the range will depend on the initial energy and charge of the ionising particle, as well as on the nature and density of the absorber medium.

Charged light particles

The charged light particles, i.e. the β-particles, will interact differently with the absorber atoms. The reason is found in their mass; it is equal to the mass of the orbital electrons, such that it can lose a significant portion of its energy in a single interaction. This, combined with the stochastic nature of the interactions, will lead to a large variation in stopping power and range of β-particles. Furthermore, they will not only lose energy through coulomb interactions, but also due to radiative losses, such as bremsstrahlung, as discussed earlier. As such, there are two components to the stopping power that were also calculated by Bethe: the collisional part S_c and the radiative part S_r. S_c does not differ very much from eq. (2.15) - apart from some correction terms - such that $S_c \sim \frac{NZ}{E} \ln \frac{E}{I}$. The radiative part is given by

$$S_r = \frac{NEZ(Z+1)e^4}{137 m_e^2 c^4} \left[4 \ln \left(\frac{2E}{m_e c^2} \right) - \frac{4}{3} \right]. \tag{2.16}$$

The total linear stopping power is then defined as the sum, so that $S = S_c + S_r$. [25] Because of the large variation in stopping power, the ranges of β-particles are determined experimentally, in the same setup as for the heavy charged particles. An empirical formula for the range of a β-particle with initial energy E_0 (in keV) in a medium with density ρ in g/cm^3 is

$$R = \frac{K}{\rho} E_0^{\gamma}. \tag{2.17}$$

With $K = 1.64$ [/] and $\gamma = 1.2 - 1.7$ [/] giving the best agreement with experimental results. [22] Figure 2.8 gives the range of common charged ionising particles in relevant media. A key point of this graph is the fact that the range of β-particles usually is at least an order of magnitude larger than the range of α-particles.

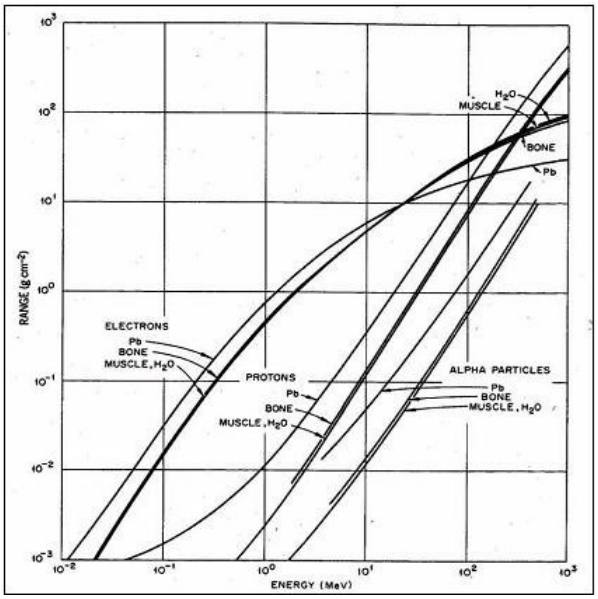

Figure 2.8: Range of different charged ionising particles times the density of the respective media. [31]

The above results have been calculated for electrons, but it should be noted that positrons will show almost exactly the same behaviour. This is because electrons and positrons have the same mass and their charge is equally large in magnitude, but opposite in sign. The main difference is the fact that positrons will undergo positron annihilation once they are stopped. The interaction of the annihilation photons with the environment is the subject of the next part.

2.2.2 Neutral particles

Neutral particles interact very differently compared to charged particles, because there is no coulomb interaction involved. In contrast with charged particles, which ionise the environment directly, the ionisation of the atoms by neutral particles will happen indirectly in two steps. First the ionising particle will interact with the orbital electrons (in the case of photons) or with the atomic nucleus (in the case of neutrons) and will consequently produce secondary charged radiation, that will ionise the atoms as discussed in the previous part. [32]
There are three mechanisms for photons and electrons to interact, figure 2.9 shows the relative importance of each interaction depending on the photon energy and the atomic number the absorber. The lines indicate where the cross sections[2] of the two adjacent interactions are equal.

[2]Comparing cross sections of interactions is the same as comparing their relative likelihood of occurence. [5]

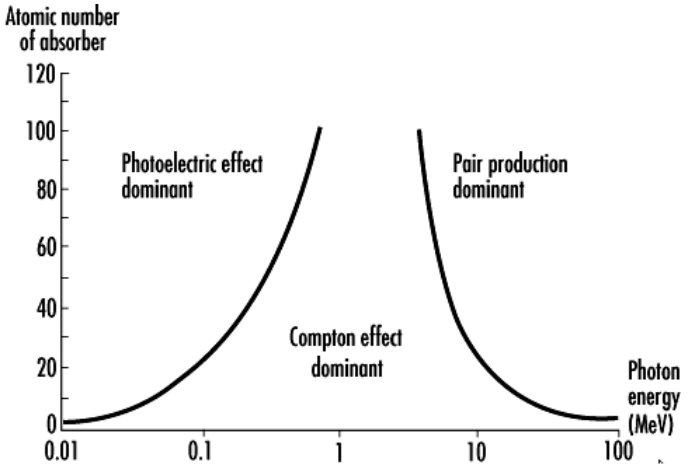

Figure 2.9: Relative importance of the three photon interactions with electrons. [30]

Photoelectric effect

For low energy photons in high Z absorber materials the photoelectric effect is the dominant interaction. This effect was first explained by A. Einstein in 1905. [33] An incoming photon with energy E_γ will interact with an orbital electron with binding energy E_b, resulting in its emission. From conservation of energy, the energy of the emitted electron is

$$E_{e^-} = E_\gamma - E_b. \tag{2.18}$$

The cross section σ_p of the photoelectric effect is the highest for the inner K-shell of atoms; this is also where the electrons have the highest binding energy. Furthermore, it is found that

$$\sigma_p \propto \frac{Z^n}{E_\gamma^{3.5}}, \tag{2.19}$$

with n having a value varying from 4 to 5. [34] Apart from the emitted electron, another form of secondary ionising radiation will be produced. The electron vacancy will be filled by capturing a free electron, or by rearranging the electronic structure of the atom. In this process, as previously discussed, a characteristic X-ray or an Auger electron will be emitted. [25]

Compton scattering effect

Compton scattering, named after its discoverer in 1923 A.H. Compton [35], is the dominant effect in low Z absorber materials. In this reaction a photon will scatter inelastically with an electron, so that the energy and momentum of both particles change. Figure 2.10 gives a drawing of this process. The photon with initial energy E_i will be deflected at an angle θ relative to its original path of motion, while its energy will change to E_f. Assuming the struck electron is originally at rest and using conservation of energy, the energy of the electron after the collision is

$$E_{e^-} = E_i \frac{\alpha(1-\cos\theta)}{1+\alpha(1-\cos\theta)}, \tag{2.20}$$

with $\alpha = \frac{E_i}{m_e c^2}$. From this equation, it follows that the energy transferred to the electron depends on the scattering angle. E_{e^-} reaches a maximum when $\theta = 180°$. [34]

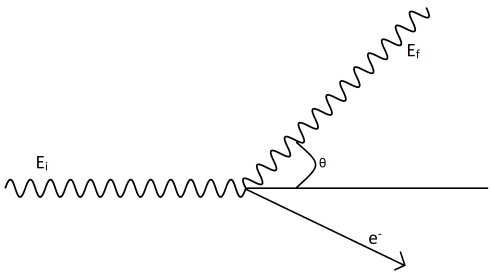

Figure 2.10: A graphical representation of Compton scattering.

A quantum mechanical derivation of the differential cross section for Compton scattering was made by Klein and Nishina. The important conclusion from the Klein-Nishina formula is the fact that the differential cross section is proportional to Z and inverse proportional to the photon energy. [36]

Pair production

In pair production the travelling photon is transformed into an electron and its antiparticle; a positron:

$$\gamma \rightarrow e^- + e^+. \tag{2.21}$$

Because the rest mass of both the electron and positron is 511 keV/c^2, reaction (2.21) is only possible when the photon energy exceeds 1022 keV. As can be seen from figure 2.9, pair production is only the dominant process at high photon energies in high Z materials. A conceptual example of how a high energy photon will deposit its energy in matter is as follows. First, pair production will occur. When the created positron comes to rest, it will produce annihilation radiation. These photons will then lose energy through Compton scattering, until they are finally completely absorbed due to the photoelectric effect. [37]

Attenuation, absorption and buildup

Consider a monoenergetic one-dimensional (narrow) photon beam travelling through a medium with thickness x. After the medium an ideal detector is placed that counts the amount of photons $I(x)$. If the original amount of photons was I_0, it holds that

$$I(x) = I_0 \mathrm{e}^{-\mu x}. \tag{2.22}$$

μ is called the linear attenuation coefficient. It is usually expressed in cm^{-1}. It is defined so that $e^{-\mu x}$ is the probability for a photon to traverse a medium of thickness x [cm] without interacting with the environment. As a consequence, the attenuation coefficient carries a contribution from all three photon interactions, as can be seen in figure 2.11. While pair production and photoelectric absorption will completely remove the photon, Compton scattering will just redirect it. If the target has a density ρ, the mass attenuation coefficient is defined as μ/ρ, expressed in cm^2/g. [38]

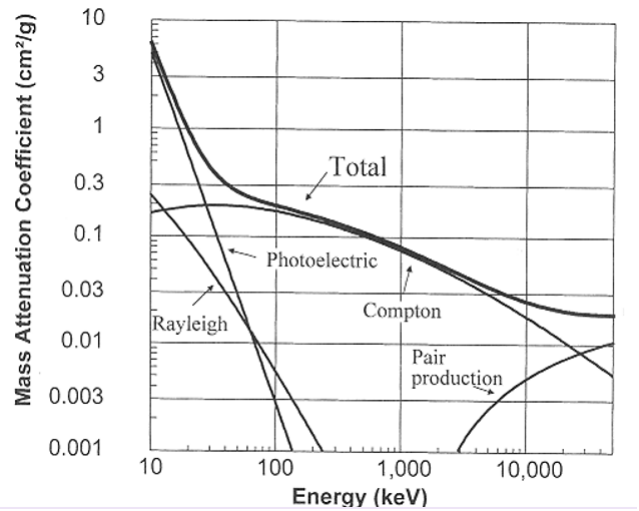

Figure 2.11: Mass attenuation coefficient as a function of photon energy in soft tissue. [32]

The attenuation coefficient describes the energy lost by the photon beam. However, a more interesting quantity is the energy deposited in the medium. For this the linear absorption coefficient is defined as μ_{en}. After rescaling with the density one finds the mass absorption coefficient as μ_{en}/ρ. This coefficient takes into account the deposited energy from electrons and positrons produced, or redirected by the photoelectric effect, Compton scattering, and pair creation. Energy deposited as a consequence of Compton scattered photons, bremsstrahlung, or annihilation radiation is not taken into account. [39]

When the conditions of a narrow beam in a thin medium no longer hold, effects of secondary radiation become more important. The exponential decay of the intensity described in eq. (2.22) no longer holds. Secondary radiation, produced by Compton scattering, will also start to reach the ideal detector, leading to an increase in detected particles. The severity of this effect depends on the thickness of the target and the initial photon energy E_γ and is described by the buildup factor $B(x, E_\gamma)$, so that (2.22) becomes

$$I(x) = I_0 B(x, E_\gamma) \mathrm{e}^{-\mu x}. \tag{2.23}$$

The effect is most important in the lighter, low Z materials. This is because the secondary photons - which are lower in energy than the primary photons - have a higher probability to undergo photoelectric absorption in high Z materials. [40]

Neutrons

Just like photons, neutrons are neutral particles, so they will not interact through coulomb forces. Furthermore, as opposed to photons, neutrons will not interact with electrons.[3] As a consequence, neutrons are only able to interact with atomic nuclei through the nuclear force. When a neutron interacts with a nucleus, three things can happen: elastic scattering, inelastic scattering or a nuclear reaction. If a neutron scatters elastically with a nucleus, total kinetic energy is conserved, so that no secondary radiation is produced.

[3] In reality there will be some electromagnetic interaction, because the neutron has a spin, magnetic moment and is composed of charged particles (quarks). However, this interaction is negligible.

This interaction is most likely to happen for neutrons of low energy, simply because they do not possess enough energy to excite the nucleus. Elastic scattering will dominate until the neutrons reach thermal energy of 0.025 eV. In inelastic scattering the neutron will leave the nucleus in an excited state; this is therefore only possible for neutrons with a sufficiently high energy. The nucleus will consequently deexcite and produce a characteristic photon as secondary radiation. In the third possibility a thermal neutron will be absorbed by the nucleus. This is most commonly followed by the emission of a proton, an α-particle or nuclear fission. [25]

2.3 Biological Effects of Ionising Radiation

2.3.1 Interaction of ionising radiation with human tissue

The basic building block of every living organism is called the cell. Small bodies, called chromosomes, are located in the nucleus of every cell. A chromosome itself consists of two molecules - also called strands - of DeoxyriboNucleic Acid (DNA) which form a helix structure. As previously discussed, ionising radiation can change the chemical interactions of matter by ionising it. When ionising particles pass through a cell, it is possible that they cause either single-strand breaks or double-strand breaks in the chromosomes. A representation those two types of strand breaks is found in figure 2.12. Three possible things can happen after a strand break. First of all, the DNA may repair itself, so that there are no detrimental effects. Secondly, the DNA may repair itself incorrectly. When a cell reproduces, an exact copy of the chromosomes of the original cell is being made. This means that if DNA is repaired incorrectly, a so-called mutation in the reproduced cells may occur. Those effects are categorised under the genetic effects. The final possibility is that the DNA is not able to repair itself. In that case the cell will die. If too many cells in one organ die, it will cause the death of the organ. This may then even result in the death of the organism itself. [41]

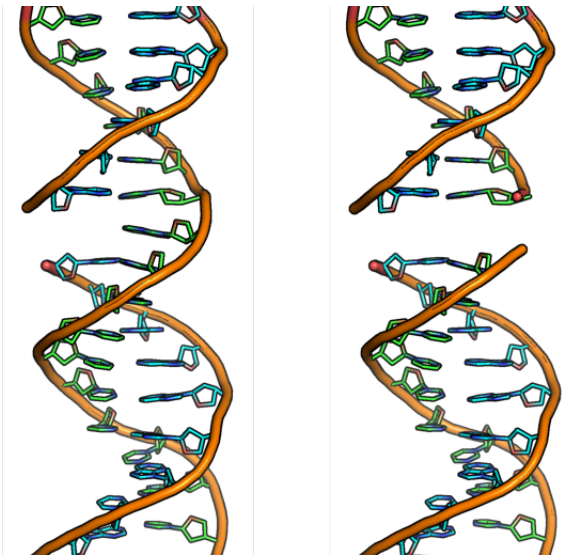

Figure 2.12: LEFT: DNA single-strand break. RIGHT: DNA double-strand break. [42]

Ionising radiation can damage DNA in a direct way or in an indirect way. In a direct way

the radiation will simply ionise the DNA and subsequently cause damage. In the indirect way the radiation will induce chemical changes in the water surrounding the DNA, which will consequently cause damage to the DNA itself. To understand this, consider radiation travelling through an ensemble of water molecules H_2O. Due to various inelastic scattering procedures multiple excited (H_2O^*) and ionised (H_2O^+) water molecules will be produced. The excited water molecule will either get rid of the excited electron, so that the molecule becomes ionised, or it will undergo molecular dissociation in the following way

$$H_2O^* \rightarrow H\cdot + OH\cdot . \tag{2.24}$$

Both reaction products are radicals; this is a molecule with an unpaired electron in its valence orbital, so that it is highly reactive. Ionised molecules will react with normal water molecules to form a hydronium ion and a hydroxyl radical.

$$H_2O^+ + H_2O \rightarrow H_3O^+ + OH\cdot . \tag{2.25}$$

It is the hydroxyl radical that will consequently interact with the DNA, causing it damage. Depending on the energy and intensity of the ionising radiation the effects will either be deterministic or stochastic in nature. Both cases will be discussed, with a focus on humans. [38]

2.3.2 Deterministic effects

Above a certain threshold of energy and intensity of radiation enough cells will be damaged so that they are not automatically repaired anymore. Not all organs are equally sensitive to radiation. The law of Bergonie and Tribon [43] gives the following three criteria for high radiosensitivity:

- organ cells have a high division rate;
- organ cells have a long dividing future;
- organ cells are of an unspecialised type.

Depending on the exposure type, deterministic effects include reddening of the skin, hair loss, nausea, damage to the offspring, and even death. While deterministic effects are severe, they have also been well studied, thanks to historical events. The most important data source are the survivors of the atomic bomb strikes in Hiroshima and Nagasaki. Radiation doses, mortality rates and medical records are well documented for approximately 120,000 persons involved. Other sources include the radium painters of the 1920's, who mixed radium with fluorescent materials to paint watch dials, uranium miners, and victims of accidents. [38, 39, 44]

2.3.3 Stochastic effects

While deterministic effects happen shortly after the irradiation ($<$ 1 month) and are unmistakably the consequence of radiation, the same cannot be said for stochastic effects. The latter can occur at lower exposures, after a much longer time and - as the name suggests - it may not even occur at all. They can occur after acute exposures that also

induce deterministic effects, or can be the consequence of chronic exposure to radiation. The two most important stochastic effects for which ionising radiation is proven to be accountable are genetic effects and carcinogenesis[4]. The main problem in evaluating the stochastic effects is finding the probability of causation. Besides the exposure to radiation, the probability that an individual will develop a form of cancer will also depend on his/her age, gender, exposure to other carcinogens, lifestyle, etc. The probability that a developed cancer is caused by a specific carcinogen is proportional to the radiation dose. [32, 45] At high doses, the development of cancer caused by radiation is well known, because the effects are deterministic and there is a lot of data available, as previously discussed. Because there is not enough data in the low dose region, data from high doses can be extrapolated to low doses, to estimate the risks associated with them. This will lead to different models. Figure 2.13 shows different means of extrapolation. The model used in regulation is the Linear No-Threshold Model (LNT), which assumes a linear relation between risk and dose, and assumes risk even at the smallest doses. The linear threshold model does not assume this last part; a certain dose has to be exceeded to have a form of risk. The hormesis model even assumes that low doses are associated with lower cancer risk than no dose at all. [46] The other models are based on various mathematical models of cancer risk. [39]

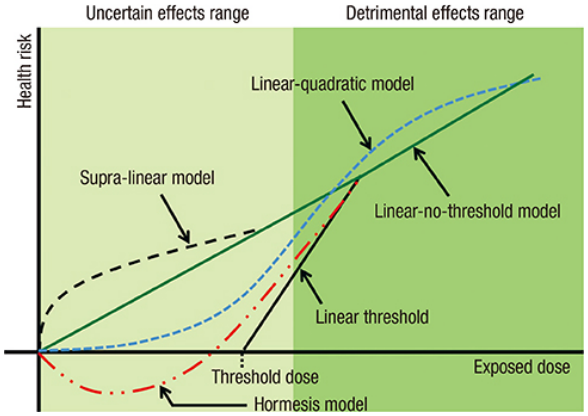

Figure 2.13: Different methods of extrapolation from deterministic data. [47]

2.4 Radiation Dosimetry

In order to quantify the notion of risk, discussed in the previous section, some physical definitions need to be provided for concepts such as exposure or dose. Historically this has been the work of the International Commission on Radiation Units and Measurements (ICRU) and the International Commission on Radiological Protection (ICRP).[5] The definition of these quantities is based on the biological effects of ionising radiation.

[4]Formation of cancer.

[5]Originally these commissions were founded under another name, but for the sake of clarity and consistency only their current names will be used.

2.4.1 Exposure

Exposure is a unit defined for photon radiation in air only. When the ionising photons travel through air, they will ionise it. The resulting ions are charged and this charge can be measured. Exposure is then defined as the total charge of the produced ions per unit mass, so that its SI unit is C/kg. In most tables, however, exposure is expressed in Roentgen (R)[6]. While not being applicable in a lot of situations, it gives a first example of a quantitative measure of radiation effects.

2.4.2 Absorbed, equivalent and effective dose

Absorbed dose

While exposure gives a measurable and practical measure for the amount of gamma radiation present in air, it is desirable to know how much of any type of radiation is absorbed in any medium. For this reason, the absorbed dose D is defined.

$$D = \frac{d\epsilon}{dm}. \tag{2.26}$$

Here $d\epsilon$ [J] is the energy absorbed by the medium with a mass dm [kg]. The SI unit of absorbed dose is the gray (Gy), which is defined as 1 Gy = 1 J/kg. Sometimes instead of absorbed dose, Kinetic Energy Released Per Unit Mass (Kerma) is used, which is defined as

$$\text{kerma} = \frac{dT}{dm}, \tag{2.27}$$

where dT [J] stands for the kinetic energy transferred to particles in the medium of mass dm. Kerma also has the unit gray. The quantities are more or less the same at low energies, but at high energies kerma will be higher, because energy losses due to bremmsstrahlung are not accounted for in absorbed dose. [39]

Equivalent dose

The Linear Energy Transfer (LET) describes the energy a particle deposits in a medium along its track. Since heavy charged particles like protons and α-particles have the highest probability of interacting with the medium, they have a higher LET than lighter particles such as electrons. A higher LET will consequently lead to more severe biological damage. To take into account the fact that different types of radiation will have different biological effects, the equivalent dose is defined as

$$H_T = \sum_R w_R D_{T,R}. \tag{2.28}$$

The summation happens over all types of radiation present. w_R is a dimensionless radiation weighting factor, whose current values are defined in the ICRP 103 report. [48] Equivalent dose has the same dimension as absorbed dose [Gy], but is expressed in sievert (Sv) to avoid confusion. Table 2.1 gives the most current values of the weighting factors

[6] 1 R = 2.58 $\times 10^{-4}$ C/kg.

for different types of particles. Because the neutron interaction depends heavily on the neutron energy, the neutron weighting factors are energy dependent as seen in figure 2.14.

Table 2.1: Weighting factors of different types of radiation as recommended by ICRP 103.

Radiation type	w_R
Photons	1
Electrons and muons	1
Protons	5
α-particles and heavy nuclei	20

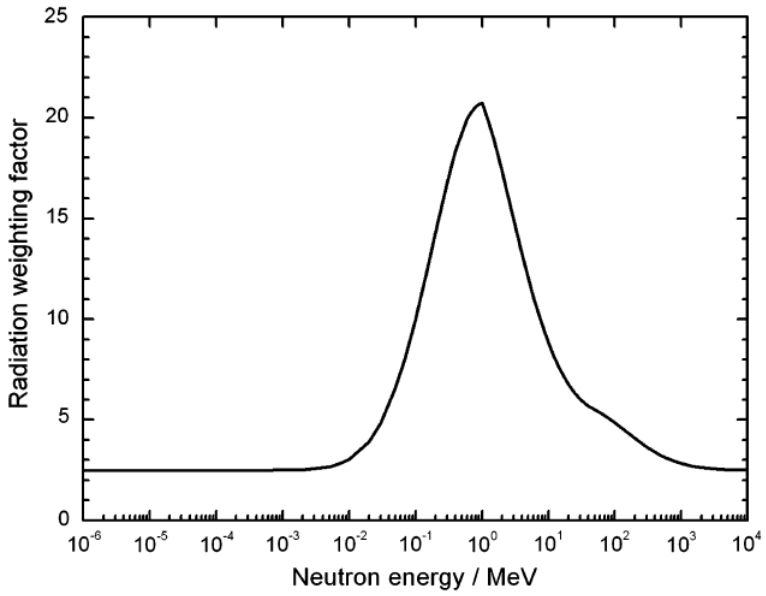

Figure 2.14: Neutron weighting factors versus neutron energy.

Effective dose

According to the law of Bergonie and Tribon, different organs will have a different sensitivity to radiation, depending on the type of cells that constitute it. To account for this, ICRP 103 also defined weighting factors w_T for different organs and defined the effective dose E [Sv] as

$$E = \sum_T w_T \sum_R w_R D_{T,R}. \tag{2.29}$$

Table 2.2 gives the different weighting factors. Notice that for whole body exposure the effective dose equals the equivalent dose, since $\sum_T w_T = 1$. [32]

Table 2.2: Weighting factors of different organs as recommended by ICRP 103.

Organ	w_T
Bone marrow Breast Colon Lung Stomach	0.12
Gonads	0.08
Bladder Liver Oesophagus Thyroid	0.04
Skin Bone surface Brain Kidney Salivary glands	0.01
Remainder	0.12

2.5 Medical Applications of Tb Isotopes

2.5.1 Diagnostic nuclear medicine

Since X-rays are weakly attenuated in soft tissue but strongly attenuated by bones, it was found, soon after their discovery in 1895, that they could be used to form images of the human skeletal structure. Since then, after the discovery and origin of different types of radiation, various imaging techniques have been invented, leading to an important application of ionising radiation still used today: diagnostics. Not all imaging techniques will be discussed, but rather those that are relevant in the context of terbium. [5]

PET

In Positron Emission Tomography (PET) β^+-emitters are used. A biologically active molecule is induced in the part of the body under examination. In this molecule one chemical element is replaced by a radioactive isotope, called the tracer. This process is known as labelling. In the case of PET imaging, the isotope will be a β^+-emitter. The resulting molecule is known as a radiopharmaceutical. The emitted positrons will annihilate after the interaction with electrons and subsequently produce two annihilation photons moving in opposite directions. These photons will be detected in coincidence, so that with a large number of detections, it is possible to reconstruct the distribution of the radioactive tracers. The most common tracers include radioisotopes of bio-elements, such as ^{15}O ($T_{1/2}$ = 2.03 min), ^{13}N ($T_{1/2}$ = 9.96 min) and ^{11}C ($T_{1/2}$ = 20.4 min). These can be used to replace elements in almost all biologically active molecules, such as the

amino acids or glucose. Furthermore, other elements such as ^{18}F ($T_{1/2}$ = 109.7 min) and ^{124}I ($T_{1/2}$ = 99.6 h) are used, because of their chemical similarity to the bio-elements. Their longer half-life also permits to evaluate biological processes that take longer than the short half-lives of the bio-elements. [49]

SPECT

The main idea behind Single Photon Emission Computed Tomography (SPECT) is the same as for PET scanning. The tracers are now radioisotopes that emit γ-rays directly. The single photons emitted are consequently detected with an Anger camera. This camera uses the principle of collimation to detect only γ-rays that travel perpendicularly to the detector. A high Z material such as lead is used for the collimation, since it is a good attenuator for γ-rays. In the perpendicular direction holes are made in the material so that only perpendicular photons will pass and be detected, usually by an inorganic scintillator. [50] Commonly used isotopes for this imaging technique include ^{99m}Tc ($T_{1/2}$ = 6.02 h, E_γ = 142 keV), ^{131}I ($T_{1/2}$ = 8.03 days, E_γ = 364 keV), ^{123}I ($T_{1/2}$ = 13.2 h, E_γ = 159 keV) and ^{111}In ($T_{1/2}$ = 2.8 days, E_γ = 171, 245 keV). [51]

2.5.2 Therapeutic nuclear medicine

The biological effects of ionising radiation can also be sought out deliberately. By irradiating tumor tissue and consequently causing double stranded breaks in the DNA, there will be a great reduction in the bad tissue. [52] Furthermore, tumor tissue is less capable of self-repairing compared to healthy tissue. However, to minimise detrimental effects to healthy tissue and maximise the dose deposited in the tumor tissue, low-range particles with a high LET such as α- and β-particles should be used for treatment purposes. Radioisotopes should be chemically implanted on biologically active molecules, just like in nuclear imaging. Consequently, they are to be transported to the tumor tissue, where they will decay and damage the bad tissue. [53] The similarities between the introduction of radioisotopes for imaging and therapeutic use, has created a whole new field in nuclear medicine: theranostics. By binding chemically similar isotopes used for both imaging and therapy to a radiopharmaceutical, diagnosis and treatment of cancer can be combined. This can be very time-efficient and cost-reducing and can also greatly reduce the radiation the patient is exposed to. [54]

2.5.3 Tb isotopes

Being a unique case, the lanthanide terbium has four different isotopes that are interesting in nuclear medicine applications. Table 2.3 gives a summary of those four isotopes and their main applications. ^{149}Tb emits α-particles with an energy of 3.967 MeV, making it the only radioisotope with a suitable half-life in the lanthanide group for α-therapy. ^{152}Tb will emit positrons with an energy of 1.08 MeV, making it, along with its relatively long half-life for a β^+-emitter, a suitable candidate for PET imaging. ^{155}Tb will emit γ-rays with energies of 86.55 keV and 105.3 keV after electron capture, making it suitable for SPECT imaging. Finally, ^{161}Tb will emit β^--particles with an average energy of 0.154 MeV along with Auger electrons, making it a useful isotope for β^-- and Auger therapy.

Table 2.3: Tb isotopes with their main properties and possible applications.

Isotope	decay mode	$T_{1/2}$	application
^{149}Tb	$\alpha(16.7\%)$	4.12 h	α-therapy
^{152}Tb	$\beta^+(17\%)$	17.5 h	PET
^{155}Tb	EC(100%)	5.32 d	SPECT
^{161}Tb	β^-	6.89 d	β^-/Auger therapy

Because all Tb isotopes have the same chemical properties, they can all bind to the same biological molecules, making it very suitable for theranostic purposes. Figure 2.15 gives the chemical structure of terbium-cm09, a molecule that is used for targeting cancer cells. The black part is a folic acid that functions as the targeting agent and will bind to the tumor cells. The green part is an albumin-binding entity which prolongs the biological half-life in the blood to match the physical half-lives of the isotopes. Finally, the red part is a DOTA chelator, which is used to label the molecule with terbium. [55]

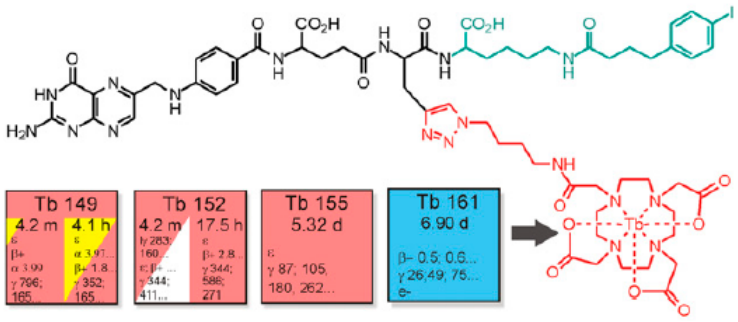

Figure 2.15: Chemical structure of terbium-cm09.

3 | Regulation

Ever since the first discovery of the detrimental effects of ionising radiation, it has been clear that there is a need for regulation on the use of radioactive materials. The various advisory and regulatory bodies that were created to this end - with a focus on Europe - will be discussed in this chapter. Afterwards, the general philosophy and working principles of the regulation that were created by these organisations are explained. To finish, the regulation on nuclear transport in Belgium will be introduced. The sole focus will be on the theoretical calculations needed to establish the regulations, rather than on the practical implementation.

3.1 Regulatory bodies

The regulations about ionising radiation have been established through a combination of fundamental scientific research and legislative expertise. Building a bridge between the very different disciplines involved has lead to a complex entanglement of regulatory bodies. In this section the most important bodies involved in the creation of regulation in Belgium are discussed. Typically, scientific bodies such as the United Nations Scientific Committee on the Effects of Atomic Radiation (UNSCEAR) or the Committee on the Biological Effects of Ionizing Radiation (BEIR) publish new insights or results from fundamental research. Based on these publications, the ICRP compiles new recommendations on radiation protection in a report. International legislative bodies such as the International Atomic Energy Agency (IAEA) or European Atomic Energy Community (Euratom) propose new regulations based on the ICRP recommendations. These regulations are then reviewed by national agencies, so that they can propose regulations for the specific country. In Belgium this is done by the Federaal Agentschap voor Nucleaire Controle (FANC)[1]. [44] A schematic overview of the regulatory process can be found at the end of this section in figure 3.1.

UNSCEAR

The UNSCEAR was founded in 1955 during a General Assembly of the United Nations. Its foundation was a response to concerns about ionising radiation in a time when nuclear weapons were being tested abundantly. [39] At the moment of writing this, 27 nations participate in UNSCEAR meetings. All nations with a considerable nuclear weapon arsenal are included. Belgium is also one of the 27 participants. Every five to fifteen years UNSCEAR reviews the latest scientific literature and publishes reports which will form

[1] Federal Agency for Nuclear Control.

the scientific fundamentals of the regulation. [44] It should be noted that UNSCEAR only evaluates scientific consequences of ionising radiation. It will not take into account socioeconomic or political factors, nor will it provide any (guidance on) regulation. [56]

ICRP

The ICRP was founded in 1928, originally out of concern of detrimental effects of radioactivity used in the medical world. The ICRP is an independent commission that publishes recommendations concerning radiation protection in its own scientific journal: Annals of the ICRP. [57] The recommendations are based on previously published scientific work from bodies like UNSCEAR. [44] While regulations published by the ICRP are recommendations and therefore not binding, the legislative bodies of most countries base their regulations entirely on the ICRP recommendations. [39] The ICRP consists of four committees, each with a different speciality [58]:

- **Committee 1: radiation effects**. This committee considers all possible biological effects of ionising radiation.
- **Committee 2: doses from radiation exposure**. The second committee is concerned with the assessment of radiation exposures, both internal and external.
- **Committee 3: radiological protection in medicine**. The third one deals with the protection of patients and staff in the medical community.
- **Committee 4: application of the commission's recommendations**. The fourth committee advises people on how the ICRP recommendations are best applied in practice.

IAEA

The IAEA was founded in 1957 as an autonomous organisation. It originates from U.S. President Eisenhower's "Atoms for Peace" speech during the General Assembly of the United Nations. The purpose of the IAEA is twofold. First of all, it promotes the safe and peaceful use of nuclear energy. Secondly, IAEA ensures non-proliferation by imposing strict rules on the use of fission materials. [59] The reports published by IAEA are based on the ICRP recommendations. U.N. member states are not obligated to follow IAEA regulations, but some repercussions, such as loss of nuclear research subsidies may happen. Some regulations may even be legally enforced by the U.N. [39]

Euratom

The Euratom, also founded in 1957, can be considered the European counterpart of the IAEA. It is officially independent from the European Union, but does have the same member states. Euratom also publishes regulations on nuclear safety and the peaceful application of nuclear energy. It furthermore actively prevents abuse of fission materials for military purposes with so-called safeguards. Euratom publishes regulations based on ICRP recommendations, but contrary to IAEA regulations, Euratom regulations are binding for all members; nations are allowed to enforced stricter laws, but they must be conform with the ones provided by Euratom. [44] Since IAEA and Euratom share a lot of

(European) members, the two organisations work closely together. Both also function as an international safeguards organisation with Euratom being the only one with jurisdiction concerning non-proliferation in member states of the European Union. [60]

ICRU

The ICRU was first conceived in 1925. It has been a permanent commission since 1953. The purpose of the ICRU is to construct an internationally accepted framework for the evaluation of ionising radiation data. Included in this evaluation is that of the application of ionising radiation in the medical world, the definitions of radiation-related quantities, and different measurement procedures. In cooperation with the ICRP, the ICRU has developed the previously discussed system of absorbed, equivalent and effective dose. [61]

FANC

The legislative body in Belgium is called the FANC. It is a part of the Federal Government Service of Home Affairs. FANC bases its regulations on the rules imposed by the IAEA and Euratom; the regulations are executed by the *Algemeen Reglement op de Bescherming van de bevolking, van de werknemers en van het leefmilieu tegen het gevaar van Ioniserende Stralingen (ARBIS)*[2]. FANC is mandated with three tasks [44]:

- **Nuclear safety**: perform inspections on all nuclear installations in Belgium, such as power plants.
- **Radiation protection**: ensure the safe usage of ionising radiation.
- **Non-proliferation**: guiding the inspectors of Euratom during inspections on fission materials.

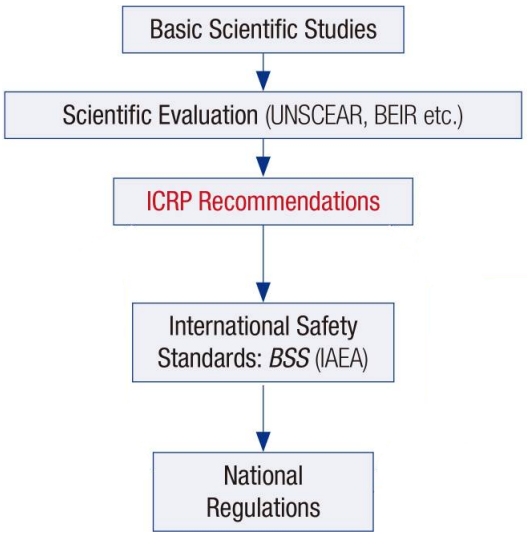

Figure 3.1: The structure of different advisory and regulatory bodies. [62]

[2]General Regulations on the Protection of the Population, Employees and the environment against the dangers of Ionising Radiation.

3.2 ICRP recommendations

As previously discussed, the entire regulation on ionising radiation originates from the recommendations of the ICRP. In first years after its foundation, ICRP focused on the deterministic effects of radioactivity. The first ICRP publication in 1928 recommended that annual doses of 1000 mSv should not be exceeded. [63] As more scientific information came to light about the stochastic effects of ionising radiation, ICRP cast aside the maximum allowed annual doses and introduced the basic principles in ICRP 26 (1977). [64] These will be discussed further on.
ICRP defines three possible ways of radiation exposure:

- **Professional exposure**: radiation exposure on the job.
- **Medical exposure**: radiation exposure of patients and people (friends, family) supporting them. The exposure of medical professional is treated as professional exposure.
- **Population exposure**: all other ways of radiation exposure of people.

Furthermore ICRP considers two different activities that lead to radiation exposure:

- **Actions**: These consist of all human activities that increase the radiation level. Action may include medical applications, storage of nuclear waste, or the nuclear fuel cycle.
- **Interventions**: These consist of all activities that are needed to decrease the radiation level. Interventions are needed during nuclear incidents or when an existing radioactive source needs to be removed.

The basic principles of ICRP try to be as general as possible, but some distinction is made between different ways of exposure and different types of activities. [44]

3.2.1 ICRP basic principles

Since ICRP 26 (1977) there are three basic principles: optimisation, justification and dose limits. The most current version from ICRP 103 will be discussed. [48] These recommendations are completely adapted in Euratom Basic Safety Standard Directive 2013/59. As of February 2018, all member states have conformed to those rules. [65]

Justification

As the name suggests, activities that involve ionising radiation should be justified. The main guideline is that the advantages should outweigh the disadvantages. More specifically, by increasing the radiation level, or by trying to decrease the (potential) exposure, there should be a sufficient personal or social benefit associated with the actions or interventions. For this reason, the irradiation of jewellery or performing radiological examinations on healthy persons, who are not in a certain risk group, are not allowed. An important remark is the fact that the person who incurs damage and the one that benefits should not be the same person. [48]

Optimisation

After an application of ionising radiation has been justified, the so-called ALARA-principle (As-Low-As-Reasonably-Achievable) has to be followed. In other words, during an activity for which the total benefits outweigh the disadvantages, the margin between the two must also be kept as large as possible. This must be done without needlessly increasing the (monetary) cost for very little additional benefit. [48] ICRP 26 even suggests using an economic cost-benefit analysis. [64] Figure 3.2 represents such an analysis graphically. It is clear that the protection cost increases if the collective dose is reduced. In the region of very low doses, reducing the dose even further will become increasingly expensive. The dose cost in the graph is a monetary value associated with a certain dose. [44]

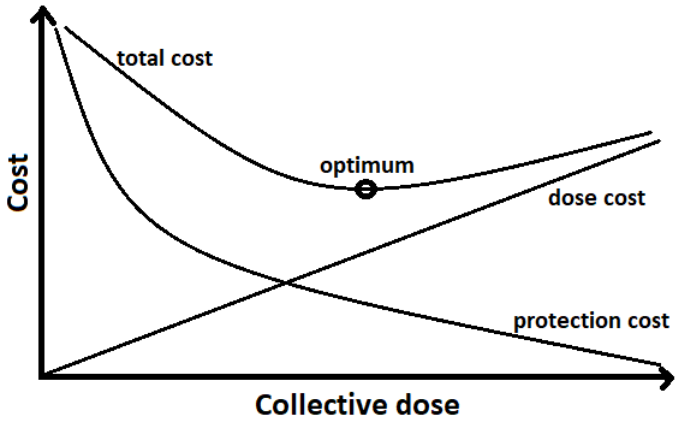

Figure 3.2: Cost-benefit analysis for the optimisation principle.

Dose limits

Following the justification and optimisation principle, it might still be the case that one individual may receive a very high dose, justified by a high social benefit or benefit for another individual. For this reason, dose limits have been introduced. Table 3.1 gives the equivalent dose limits for professionals[3] and for the public, as determined in ICRP 60 but still valid in ICRP 103. Dose limits do not apply for medical use, interventions, potential exposure and, Naturally Occurring Radioactive Material (NORM).

Table 3.1: Annual ICRP dose limits .

Limit type	Professionals (mSv/year)	Public (mSv/year)
Effective dose	20	1
Lens of the eye	150	15
Skin	500	50
Hand and feet	500	-

The effective dose limit for professionals is a yearly average of 20 mSv over 5 years. In one year the effective dose should not exceed 50 mSv. The equivalent skin dose is averaged

[3]People who work with ionising radiation in their profession.

over an area of 1 cm^2 regardless of the area that was exposed. [48] These limits were determined by using the LNT model on estimating the cancer probability for low doses. In general, 5 %/Sv is taken as the reference value for cancer risk. The extrapolated risk for other detrimental effects is much lower, so that the value for cancer risk is adequate. [32] Furthermore, it should be noted that the annual effective dose limits for the public of 1 mSv is lower than the annual effective dose due to NORM. This dose is 2 mSv/year on a global average. [44]
On the opposite side of dose limits there is also an exemption level. Following the saying "de minimis non curat lex"[4], ICRP argues that annual doses below 0.01 mSv should be exempted from the regulation, as the detrimental effects from such low doses are negligible. [44]

3.3 Nuclear transport in Belgium

The regulation on nuclear transport in Belgium is determined by FANC and executed by ARBIS. However, FANC chooses to completely adopt the IAEA guidelines.[5] [66] Those guidelines are published in the IAEA Specific Safety Requirements, SSR-6. [67]

3.3.1 Packaging

To start with, FANC defines 5 different types of packages in which radioactive material must be transported, based on the activity and nature of both the material and the type of transport.

Exempted packages

Whenever the activity of a certain material is below a certain threshold, its dangers are considered insignificant. Consequently, exempted packages are not subject to radiation shielding requirements. Those exemption levels differ for each type of radiation. They are listed in table 3.2. Common products shipped in this type of package are radiopharmaceuticals and very small sources for industrial use. [66]

Table 3.2: Activity exemption levels.

Emission type	Exempted activity [Bq]	Exempted concentration [Bq/g]
Gamma or beta	10.000	1
Alpha	1.000	0.1
Neutron or unknown	1.000	0.1

Industrial packages

Two types of materials are shipped in industrial packages. Firstly, large volume materials that have a very low specific activity, such as hospital waste. Secondly, non-radioactive

[4]The laws does not concern itself with trifles.

[5]This is an example of the close collaboration between the IAEA and Euratom in matters that do not concern non-proliferation. Euratom has no specific publications on regulation of nuclear transport, but bases itself on the IAEA Specific Safety Requirements instead.

objects that are surface contaminated with radioactive material, such as tools used in the fuel cycle. As standard requirements, all industrial packages must remain intact in three different situations: falling from a vehicle, exposure to rain, and stabbing with a sharp object. Depending on the nature of the shipped material, IP-1, IP-2 or IP-3 packages are used. The requirements for each package on top of the standard ones is listed in table 3.3. [68]

Table 3.3: Additional resistance requirements on top of the standard requirements for industrial packages.

Package type	Requirements
IP-1	-
IP-2	Free drop (0.3 m to 1.2 m), stacking and compression
IP-3	IP-2 and penetration (6 kg steel bar dropped from 1 m)

Type A packages

Type A packages are designed to be able to safely transport radioactive sources. It must satisfy all the requirements for IP-3 industrial packages as well as provide extra shielding for ionising radiation. It is also the most commonly used package for the transport of medical isotopes. Non-irradiated fuel cycle elements are also frequently transported in these packages. [66] Only isotopes whose activity is below certain values, called the A_1 and A_2 values, are allowed to be shipped in a type A package. These values have to be determined for every radioisotope separately. The methodology of this calculation will be explained further on. [67]

Type B packages

When the activity of a radioisotope exceeds the A_1 and A_2 values, it must be transported in a type B package. It must satisfy all the safety standards required for type A packages. Furthermore, in order to ensure its survival in a severe accident, it is subject to several other requirements. First of all, it must be able to withstand a drop of a 500 kg mass from a height of 9 m. It must also be resistant to a fire of 800 °C during 30 minutes. Finally, it must endure an immersion in water at a depth of 15 m during 8 hours. In some special cases of very high activity, the immersion test must be at a depth of 200 m during 1 hour. [68]

Type C packages

While radioisotopes transported by aeroplane may travel in type A or type B packages, IAEA recommends the use of type C packages. On top of standard type A and type B requirements, type C packages must be resistant to a fire of 800°C during 60 minutes. It must also be able to survive an impact collision, travelling no less than 90 m/s. [68]

3.3.2 A_1/A_2 values: the Q system

The SSR-6 report of the IAEA defines the activity limits for radioactive transport in type A packages, called the A_1 and A_2 values. The A_1-value is valid for all special form sources. To be in a special form, the material must either be an indispersible solid, or sealed in a capsule. [69] The A_2-value is the limiting activity for open sources. [67] The actual calculation method of these values is explained in the IAEA SSG-26 report, which serves as a complementary document on the SSR-6 transportation regulations. Nuclear transport falls in the category of potential exposure. Consequently, the dose limits listed in table 3.1 do not apply. However, the IAEA chooses to base the calculations of the activity limits on the annual dose limits for exposed professionals. [70] In case of an accident, the SSR-6 report makes the following - purposely conservative - assumptions:

- The shielding of the radioactive material is completely lost.
- An exposed worker will stand at a distance of 1 m from the source.
- An exposed worker will spend no longer than 30 minutes in the proximity of the source.

Based on these assumptions, the activity of the source is limited to the value that would cause an effective whole body dose of 50 mSv or an equivalent skin dose of 500 mSv. Taking into account the fact that the exposure time is 30 minutes, the effective dose rate limit must be 100 mSv/h and the equivalent dose rate limit must be 1 Sv/h. Since the effective and equivalent dose depend highly on the radiation type and energy, calculations need to be done for each isotope separately. For the most commonly transported radioisotopes, these calculations have already been done and are listed in the SSR-6 report. [67] Isotopes for which these calculations have not been performed are subject to predetermined A_1 and A_2 values, which are listed in table 3.4.

Table 3.4: A_1 and A_2 values for isotopes that have not been studied yet.

Radiation type	A_1 [TBq]	A_2 [TBq]
Gamma or beta	0.1	0.02
Alpha	0.2	9E-5
Neutron or unknown	0.001	9E-5

The actual calculation of the A_1 and A_2 values is done using the so-called Q system. It was worked out by H.F. Macdonald and E.P. Goldfinch in 1980. [71] The Q system considers five types, each associated with a different kind of radiation exposure, labelled Q_A, Q_B, Q_C, Q_D and Q_E. They represent the activity limit concerning the exposure pathway they are associated with:

- Q_A: the activity limit due to external photon radiation,
- Q_B: the activity limit due to external beta radiation,
- Q_C: the activity limit for exposure due to inhalation,
- Q_D: the activity limit for exposure due to skin contamination or ingestion,

- Q_E: the activity limit for submersion in a radioactive gas.

A_1 is the lesser of Q_A and Q_B, while A_2 will be equal to the smallest Q value in general. In the following section all Q values will be discussed in more detail.

Q_A value

The Q_A value is the activity of a certain isotope that will lead to an effective dose rate of 100 mSv/h at a distance of 1 m, only taking into account the emitted photon radiation. Both prompt and delayed gamma rays, X-rays as well, as annihilation radiation are considered. [70] Data of emission spectra for every known isotope is found in ICRP 107. [72] Denote with $\dot{e}_{pt}$ [Sv Bq^{-1} h^{-1}] the so-called photon dose rate coefficient. It must hold that $\dot{e}_{pt} Q_A = 100$ mSv/h, or

$$Q_A[\text{TBq}] = \frac{10^{-13}}{\dot{e}_{pt}}. \tag{3.1}$$

The photon dose rate coefficient itself can be calculated with the following formula:

$$\dot{e}_{pt} = \frac{C}{4\pi d^2} \sum_i \left(\frac{e}{X}\right)_{E_i} Y_i E_i \left(\frac{\mu_{en}}{\rho}\right)_{E_i} e^{-\mu_i d} B(E_i, d). \tag{3.2}$$

Here, d [cm] is the distance from the source. The summation is done over all photon radiation values found in ICRP 107 for a particular isotope. E_i [MeV] is then the energy of that photon with yield Y_i [Bq^{-1} s^{-1}]. $\left(\frac{\mu_{en}}{\rho}\right)_{E_i}$ [cm^2 g^{-1}], μ_i [cm^{-1}] and $B(E_i, d)$ are the mass attenuation coefficient, linear attenuation coefficient and buildup factor, as discussed in chapter 2, respectively. $\left(\frac{e}{X}\right)_{E_i}$ [Sv R^{-1}] is the relationship between the effective dose and the exposure in air. Finally, $C = 6.581$ R h^{-1} g s MeV^{-1} is a unit conversion factor. [70]

Q_B value

The Q_B value is the activity that will lead to an equivalent skin dose rate of 1 Sv/h at 1 m from the source, considering only beta emission. It should be noted that all types of electrons and positrons are considered. Both those with a continuous spectrum following β-decay, as well as monoenergetic Auger electrons and electrons following internal conversion. Again, this data is found in ICRP 107. [72]
Analogous to Q_A, the equivalent skin dose rate coefficient $\dot{e}_\beta$ [Sv Bq^{-1} h^{-1}] is defined as

$$Q_B[\text{TBq}] = \frac{10^{-12}}{\dot{e}_\beta}. \tag{3.3}$$

Because beta radiation is much more easily stopped compared to gamma radiation, the assumption of complete loss of shielding is not valid in the calculation for Q_B. Instead, an extra absorber with a density of $d = 150$ mg/cm^2 is assumed. The extra shielding factor

S due to this absorber is then given by

$$S = e^{\mu d}. \tag{3.4}$$

The factor μ is determined by the empirical formula $\mu = 0.017 E_\beta^{-1.14}$. Where E_β denotes the electron energy in the case of monoenergetic electrons, and the endpoint energy in the case of a continuous β-spectrum. [70] Taking the shielding factor into account, the equivalent skin dose rate coefficient is calculated as

$$\dot{e}_\beta = \frac{J_{air} C}{S}. \tag{3.5}$$

Here, J_{air} [MeV g^{-1} Bq^{-1} h^{-1}][6] is the equivalent dose at 1 m in air. It denotes the dose due to one electron at a distance r from the source in air. For many radioisotopes J_{air} values were calculated and tabulated by Cross in 1982. [73] Furthermore, $C = 5.767 \cdot 10^{-7}$ Gy h^{-1} MeV^{-1} g s^{-1}, is a unit conversion factor. Note that, since the radiation weighting factor for β-particles is 1, absorbed dose and equivalent dose will have the same numerical value.
Furthermore, it should be noted that, as seen in table 3.1, the lens of the eye has a separate annual dose limit of 150 mSv. Despite the fact that this value is lower than the annual skin dose limit, studies on doses of the eye lens suggest that doses to the skin are always the limiting factor for energies up to 4 MeV. [64] External gamma or beta radiation are the only exposure possibilities that are considered for sealed sources. For this reason $A_1 = \min(Q_A, Q_B)$.

Q_C value

The Q_C considers the effective dose due to inhalation. Because, realistically, the entire content of the package will not be inhaled, IAEA makes two conservative assumptions. First of all, 10^{-3} of the package content become airborne. Secondly, 10^{-3} of that fraction will actually be inhaled. [70] The effective dose coefficient for inhalation e_{inh} [Sv Bq^{-1}] can then be used to calculate Q_C. The latter is defined so that $10^{-6} \cdot e_{inh} \cdot Q_C = 50$ mSv, or

$$Q_C[\text{TBq}] = \frac{5 \times 10^{-8}}{e_{inh}}. \tag{3.6}$$

The effective dose coefficients for inhalation are based on the study of the effect of ionising radiation on the respiratory tract in ICRP 66 (1994). [74] The actual coefficients are listed for every isotope in ICRP 68 (1994) [75] or in the 1996 IAEA Basic Safety Standards. [76]

Q_D value

Q_D deals with contamination of the transported radioactive material on the skin. The important factor in calculating Q_D is the equivalent skin dose rate coefficient for skin

[6] Note that MeV g^{-1} has the same dimension as Gy or Sv. J_{air} is expressed in those units, because they are cited that way in Cross et al.

contamination $\dot{h}$ [Sv TBq^{-1} s^{-1} m^2]. This coefficient gives the equivalent dose to the skin after one hour per 10^9 disintegrations on 1 m^2 of skin.[7] The IAEA makes the assumption that an employee will wash the contaminated area after a maximum of 5 h. Furthermore, the assumption is made that 10^{-3} of the entire package content will eventually find its way to the naked skin. Q_D can then be defined so that $10^{-3} \cdot Q_D \cdot \dot{h} \cdot t = 500$ mSv, with $t = 5$ h. This can be rewritten as

$$Q_D[\text{TBq}] = \frac{2.8 \times 10^{-2}}{\dot{h}}. \tag{3.7}$$

$\dot{h}$ should be evaluated at a depth of 0.07 mm in skin tissue. For skin contamination, Cross also performed calculations for various isotopes and listed them in 1992. [77]
Furthermore, it is also assumed that a person may ingest 10^{-3} of the skin contamination in a period of 24 h. However, per unit dose intake it is always the inhalation that is the limiting factor, so that calculations for dose intake via ingestion are redundant. [75]

Q_E value

When the content of the package consists of a gaseous isotope that does not become incorporated in the body, such as a noble gas, Q_E is defined as the activity limit due to submersion in the gas. IAEA assumes the gaseous content is released in a container with a volume of 300 m^3. The initial activity concentration of $Q_E/300$ m^{-3} is assumed to decay exponentially with a decay constant of 4 h^{-1}, due to air ventilation. Using these assumptions, the mean activity concentration will be $1.44 \times 10^{-3} Q_E$ m^{-3}. Furthermore, h_{sub} [Sv Bq^{-1} s^{-1} m^3] is defined as the effective dose rate coefficient for submersion so that

$$Q_E[\text{TBq}] = \frac{1.9 \times 10^{-14}}{h_{sub}}. \tag{3.8}$$

Values of h_{sub} are tabulated in the SSG-26 report for the nobles gases. [70] This concludes the five pathways considered for open sources, so that $A_2 = \min(Q_A, Q_B, Q_C, Q_D, Q_E)$.

Q_F value

When the transported isotope is an alpha emitter[8] Q_A and Q_B are not sufficient to determine the activity limit for sealed sources. To this end Q_F is - somewhat arbitrarily - defined as

$$Q_F = 10^4 Q_C. \tag{3.9}$$

When Q_F is taken into account, it holds that $A_1 = \min(Q_A, Q_B, Q_F)$.

[7] The average human has a skin surface of 1.5-2 m^2.

[8] IAEA defines an alpha emitter as a radioisotope if 10^{-3} of its decays are alpha particles, or if it decays to an alpha emitter.

4 | Calculation of Q Values for Tb Isotopes

In the previous chapter, the system of the Q values and what they stand for has been explained. In this chapter the Q values for ^{149}Tb, ^{152}Tb, ^{155}Tb and ^{161}Tb are calculated. The first part focuses on the literature used to find all the needed parameters. After that, the different interpolation methods used on tabulated parameters are explained. Finally, the results of those interpolations along with the results of the actual calculations of the Q values are presented.

4.1 Calculation methodologies

In the 1990s, the IAEA hired S. Benassai and L. Bologna as consultants to review the calculation methodologies of the different Q values. They compiled their recommendations the ANPA report (1994). [78] The ANPA report will form the fundamentals for the calculations performed in this work. As in the previous chapter, different Q values will be discussed separately. Since Tb is not a noble gas, Q_E is not considered.

Q_A value

The photon dose rate coefficient needed in the calculation for Q_A is calculated using (3.2). The distance d is set to 100 cm, according to the IAEA rules. The dose conversion factors $\frac{e}{X}$ were determined in 1987 by the ICRP in their report ICRP 51 for different photon energies. [79] The photon energies with their respective yields are compiled in the ICRP 107 for every known isotope. Both the mass absorption coefficient $\frac{\mu_{en}}{\rho}$ and mass attenuation coefficient $\frac{\mu}{\rho}$ were calculated by Hubbell in 1982. [80] The linear attenuation coefficients were then obtained by multiplying $\frac{\mu}{\rho}$ with the density of air $\rho_{air} = 1.21 \times 10^{-3}$ g/cm^3. Finally, the buildup factors are tabulated in the ANPA report.

Q_B value

While Q_A is calculated using tabulated values that are valid for all isotopes, the situation is different in the calculation of Q_B. To calculate the beta dose rate coefficient, $\dot{e}_\beta$, the equivalent dose in air J_{air} has to be known for the isotope of interest, as seen in (3.5). While values of J_{air} for some isotopes are tabulated by Cross, this is not the case for the

Tb isotopes of interest. The equivalent dose in air at a distance r [g cm^{-2}] is given by

$$J_{air}(r,E) = \frac{J_{water}(r',E)}{\eta_{air}^3 \left(\frac{\rho_{water}}{\rho_{air}}\right)^2}. \tag{4.1}$$

Here $\rho_{water} = 1$ g/cm^3. $\eta_{air} = 1.12$ is the attenuation coefficient of water relative to air. [73] r' is the water equivalent air distance:

$$r' = \frac{r}{\eta_{air}} = \frac{100 \text{ cm} \cdot 1.21 \times 10^{-3} \text{ g/cm}^3}{1.12} \approx 0.108 \text{ g/cm}^2. \tag{4.2}$$

The reason the conversion to equivalent dose in water is made, is because Cross has performed Monte Carlo simulations in 1992 to give tabulated values of J_{water} in a dimensionless form $j(r/r_E, E)$. [81]

$$j(r/r_E, E) = 4\pi\rho r^2 J_{water}(r,E)\frac{r_E}{E}. \tag{4.3}$$

Here, r_E [cm] denotes the range of an electron of energy E [MeV] in water. These values were tabulated by M.J. Berger in 1982. [82] For monoenergetic electrons (Auger and internal conversion) J_{water} can be directly calculated from (4.3). However, for the continuously distributed energies following beta emission, an integration over the entire beta spectrum is needed so that

$$J_{water}(r,E) = \frac{n}{4\pi\rho r^2} \int_0^{E_{max}} N(E) j\left(\frac{r}{r_E}, E\right)\frac{E}{r_E} dE. \tag{4.4}$$

Where $N(E)$ [/] is the intensity of beta particles with energy E [Mev]. Furthermore, $n = \int_0^{E_{max}} N(E)dE$, is also listed in ICRP 107 for every isotope. Note that $j(r/r_E, E) \approx 0$ when $r > r_E$, so that the lower limit of the integral can also be set to the energy E' for which $r = r_{E'}$. For every isotope ICRP 107 also lists the complete beta spectrum, albeit in a discrete approximation. Therefore, in practical calculations (4.4) is approximated by

$$J_{water}(r,E) \approx \frac{n}{4\pi\rho r^2} \sum_{i=1}^{N} N(E_i) j\left(\frac{r}{r_{E_i}}, E_i\right)\frac{E_i}{r_{E_i}}\Delta E_i. \tag{4.5}$$

Where $N(E_i)$ and E_i are the intensity and energy of the beta particle as listed in ICRP 107 respectively and $\Delta E_i = E_i - E_{i-1}$. As a final remark, independent of the result for the calculation, an upper limit of 1000 TBq is artificially determined for Q_B. [83]

Q_C value

Q_C does not need any study on calculation methodology as it can readily be calculated from the tabulated values in ICRP 68 and IAEA BSS 1996. A few special remarks have to be made: [83]

- If the considered isotope is a noble gas Q_C is not relevant. Q_E should be calculated

instead.

- Q_C is also artificially limited to 1000 TBq.
- If $10^{-4}Q_C$ g^{-1} is larger than the specific activity of the considered isotope, Q_C is unlimited.

Q_D value

As is the case for the beta dose rate coefficients, the skin dose rate coefficient $\dot{h}$ has not been calculated for the four Tb isotopes of interest yet. However, Cross did calculate the dose rate at different skin depths Z/r_E in 1992. [77] He considered a plane source with an area of 100 cm^2 on an air-water interface. Using Monte Carlo simulations, averaged dose rates under the centre of the plane at a depth of Z/r_E in the water are calculated. Due to their chemical similarity, water is used to approximate the structure of skin tissue. [77] The values $j(Z/r_E, E)$ are again tabulated as dimensionless factors so that

$$J(Z,E) = j\left(\frac{Z}{r_E}, E\right)\frac{E}{\rho_{water} r_E}. \tag{4.6}$$

$J(Z,E)$ is expressed in MeV g^{-1} cm^2, so that to obtain $\dot{h}$ it has to be multiplied by a factor $C = 160.2$ Sv TBq^{-1} s^{-1} g MeV^{-1}. The contribution from monoenergetic electrons can thus be calculated from (4.6), but for the skin dose rate due to beta emission, integration is needed:

$$J(Z,E) = \int_0^{E_{max}} N(E) j\left(\frac{Z}{r_E}, E\right)\frac{E}{\rho_{water} r_E} dE. \tag{4.7}$$

Using the discrete beta spectra from ICRP 107, (4.7) is approximated by

$$J(Z,E) = \sum_{i=1}^{N} N(E_i) j\left(\frac{Z}{r_{E_i}}, E_i\right)\frac{E_i}{\rho_{water} r_{E_i}}\Delta E_i. \tag{4.8}$$

Following the IAEA guidelines Z is set to 0.007 cm. Q_D can then be calculated from (3.7). [83]

4.2 Data interpolation

To calculate Q values, a lot of tabulated data needs to be consulted. Since no theoretical formula exists for most quantities, they are determined empirically for different energies and penetration depths. To determine the quantities for all energies and penetration depths, Benassai and Bologna proposed different interpolation methods, which will be explained here.

4.2.1 Chebyshev approximation

The Russian mathematician P. Chebyshev proposed a way to approximate a continuous function $f(x)$ on an interval [a,b] using a rational function in the following way

$$f(x) \approx Q(x) = s(x)\frac{p_n x^n + p_{n-1}x^{n-1} + \cdots + p_0}{q_m x^m + q_{m-1}x^{m-1} + \cdots + q_0}. \tag{4.9}$$

The function $s(x)$, which is also continuous on [a,b], and the parameters p_i, $i \in \{0, ..., n\}$ and q_j, $j \in \{0, ..., m\}$ are determined so that

$$H_Q = \max_{a \leq x \leq b} |f(x) - Q(x)| \tag{4.10}$$

reaches a minimal value H_p. Let $P(x)$ be the function that minimises H_Q. Call N the number of times $f(x) - P(x)$ reaches the value H_p, with alternating signs, on the interval [a,b]. Chebyshev then proved the following theorem: if the function can be written as

$$P(x) = s(x)\frac{a_{n-\sigma}x^{n-\sigma} + a_{n-\sigma-1}x^{n-\sigma-1} + \cdots + a_0}{b_{m-\tau}x^{m-\tau} + b_{m-\tau-1}x^{m-\tau-1} + \cdots + b_0} \equiv s(x)\frac{A(x)}{B(x)}, \tag{4.11}$$

with $0 \leq \sigma \leq n$, $0 \leq \tau \leq m$, $b_{m-\tau} \neq 0$ and $\frac{A(x)}{B(x)}$ an irreducible fraction, then $N \geq n + m + 2 - d > 0$, with $d = \min(\sigma, \tau)$. This theorem thus guarantees the existence of $P(x)$. While analytic methods exist to approximate some functions, numerical methods in the form of least-square fits to the experimental data were used in the ANPA report. This method is justified by the aforementioned existence theorem. [84]

4.2.2 Linear interpolation

While most parameters are interpolated using a (rational) polynomial based on the Chebyshev theorem, some parameters are determined using linear interpolation or bilinear interpolation.

linear interpolation

Let $f(x)$ be a quantity that depends on one parameter x. Consider a set of n experimentally obtained data points $((x_1, y_1), ..., (x_n, y_n))$. For every interval $[x_i, x_{i+1}]$, $i \in \{1, ..., n-1\}$ a first-degree polynomial $L_i(x)$ is created that contains the points (x_i, y_i) and (x_{i+1}, y_{i+1}). This means that

$$L_i(x) = \frac{y_{i+1} - y_i}{x_{i+1} - x_i}(x - x_i) + y_i. \tag{4.12}$$

$L_i(x)$ is used to approximate $f(x)$ for $x \in [x_i, x_{i+1}]$. If $x < x_1$, the interpolated value is found using $L_1(x)$. If $x > x_n$, the interpolated value is found using $L_{n-1}(x)$. [85]

Bilinear interpolation

Bilinear interpolation is the two-dimensional analogue of linear interpolation, when a parameter $f(x, y)$ has to be determined that depends on two parameters x and y. Consider

that for the parameters $(x_1, ..., x_n)$ and $(y_1, ..., y_m)$ there are $n \times m$ values $z_{i,j} = f(x_i, y_j)$ known. For every interval $[x_i, x_{i+1}] \times [y_j, y_{j+1}]$ a two-dimensional, first-degree polynomial is created

$$L_{i,j}(x,y) = \frac{1}{(x_{i+1}-x_i)(y_{j+1}-y_j)} \begin{pmatrix} x_{i+1}-x & x-x_i \end{pmatrix} \begin{pmatrix} z_{i,j} & z_{i,j+1} \\ z_{i+1,j} & z_{i+1,j+1} \end{pmatrix} \begin{pmatrix} y_{j+1}-y \\ y-y_j \end{pmatrix}. \tag{4.13}$$

For general values (x, y) with $x \in [x_i, x_{i+1}]$ and $y \in [y_j, y_{j+1}]$, the value $f(x, y)$ is then approximated with $L_{i,j}(x, y)$. [85]

4.3 Results

4.3.1 Interpolation of photon data

Absorption- and attenuation coefficients

The common logarithm of the mass attenuation coefficient $\frac{\mu}{\rho}$ is fitted with the common logarithm of the energy E, expressed in eV, with a rational Chebyshev approximation:

$$\log\left(\frac{\mu}{\rho}\right) = \frac{a_5x^5 + a_4x^4 + a_3x^3 + a_2x^2 + a_1x + a_0}{b_6x^6 + b_5x^5 + b_4x^4 + b_3x^3 + b_2x^2 + b_1x + b_0}, \tag{4.14}$$

with $x \equiv \log(E)$. The interpolation of the mass absorption coefficient is done in a similar way using the following rational function:

$$\log\left(\frac{\mu_{en}}{\rho}\right) = \frac{c_5x^5 + c_4x^4 + c_3x^3 + c_2x^2 + c_1x + c_0}{d_5x^5 + d_4x^4 + d_3x^3 + d_2x^2 + d_1x + d_0}. \tag{4.15}$$

Jones fitted equations (4.14) and (4.15) against the data found in Hubbell [80] by Jones [83] using a least squares method. The results of the fit for the attenuation coefficient is found in table 4.2 and the results for the absorption coefficient are found in table 4.1.

Table 4.1: Results of the parameters used in the interpolation of the mass attenuation coefficient.

Parameter	Value	Parameter	Value
a_0	-84.0828	b_0	14.3532
a_1	111.3816	b_1	-22.4831
a_2	-51.5158	b_2	14.7258
a_3	10.8707	b_3	-4.7476
a_4	-1.0530	b_4	0.787644
a_5	0.036271	b_5	-0.064373
		b_6	0.002140

Table 4.2: Results of the parameters used in the interpolation of the mass absorption coefficient.

Parameter	Value	Parameter	Value
c_0	179.3046	d_0	47.7859
c_1	-13.44	d_1	-40.6171
c_2	-39.6652	d_2	18.1687
c_3	12.3564	d_3	-4.1864
c_4	-1.1702	d_4	0.402538
c_5	0.019626	d_5	-0.007719

It should be noted that the coefficients have so many significant figures because they were calculated that way in the fitting procedure. Furthermore, the results were given without any statistical analysis, the reason being the fact that extreme accuracy is not required in the calculation of the Q values, since they are heavily rounded in the end. The lack of statistical information of the fit is also justified later on, when these parameters are used to calculate and compare Q values for some known isotopes.

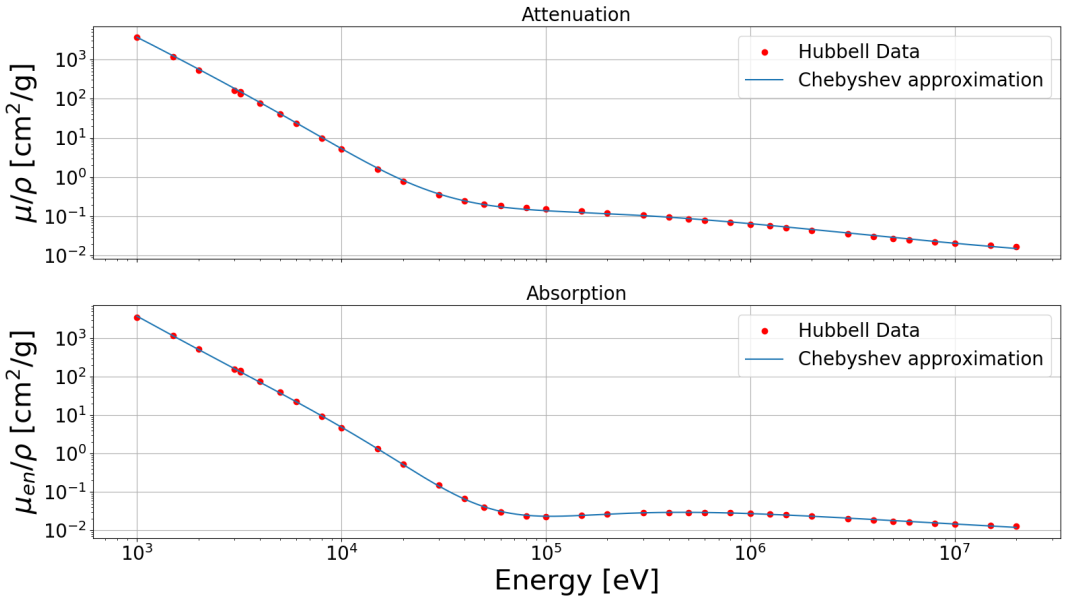

Figure 4.1: TOP: interpolation for the mass attenuation coefficient. BOTTOM: interpolation for the mass absorption coefficient.

Exposure in air to dose coefficients

The coefficients to convert exposure in air to absorbed dose $\frac{e}{X}$ are listed in ICRP 51 for energies above 10 keV. In the case of energies between 10 keV and 70 keV, the data is interpolated using the following rational function:

$$\frac{e}{X} = \frac{f_3E^3 + f_2E^2 + f_1E + f_0}{g_2E^2 + g_1E + g_0}. \tag{4.16}$$

Here E is the photon energy in MeV. $\frac{e}{X}$ is expressed in Sv R^{-1}. The fitting results of Jones are listed in table 4.3.

Table 4.3: Results of the parameters used in the interpolation of the exposure in air to dose conversion factor for energies between 10 keV and 70 keV. [83]

Parameter	Value	Parameter	Value
f_0	0.0054	g_0	101
f_1	-0.741	g_1	-3870
f_2	-12.4	g_2	87600
f_3	5430		

For energies between 70 keV and 150 keV the following polynomial is used

$$\frac{e}{X} = h_5E^5 + h_4E^4 + h_3E^3 + h_2E^2 + h_1E + h_0. \tag{4.17}$$

The results for the parameters h_0 to h_5 are found in table 4.4.

Table 4.4: Results of the parameters used in the interpolation of the exposure in air to dose conversion factor for energies between 70 keV and 150 keV. [83]

Parameter	Value
h_0	0.00724
h_1	-0.006711
h_2	0.005506
h_3	-0.001795
h_4	0.000254
h_5	-0.000013

Finally, for photon energies greater than 150 keV the same 5th degree polynomial as in eq. (4.17) is used. The fit results, however, are different than for lower energies. The results are tabulated in table 4.5

Table 4.5: Results of the parameters used in the interpolation of the exposure in air to dose conversion factor for energies larger than 150 keV. [83]

Parameter	Value
h_0	0.00059
h_1	0.00057
h_2	-0.00014
h_3	0.0000246
h_4	-0.0000016
h_5	0.00000002

Buildup factors

The last parameter needed in the calculation of Q_A is the buildup factor B. For some energies larger than 15 keV they are listed in the ANPA report. For photon energies smaller than 15 keV a buildup factor of $B = 1.05$ is assumed. Again, different fitting functions are used for different energies to interpolate the values of the buildup factor. Furthermore, the notation $x = \log(E)$ is used, where E is the photon energy expressed in MeV. For energies between 15 keV and 20 keV only two fitting parameters are needed, so that the buildup factor can be calculated as

$$\log(B) = 0.37x + 0.46. \tag{4.18}$$

For energies larger than 20 keV, a higher order polynomial is needed:

$$\log(B) = j_6x^6 + j_5x^5 + j_4x^4 + j_3x^3 + j_2x^2 + j_1x + j_0. \tag{4.19}$$

The results for this fit are found in table 4.6

Table 4.6: Results of the parameters used in the interpolation of the buildup factor for photon energies larger than 20 keV. [83]

Parameter	Value
j_0	0.0028
j_1	-0.0028
j_2	-0.0036
j_3	-0.0019
j_4	0.0122
j_5	-0.0016
j_6	-0.0042

4.3.2 Interpolation of beta particle data

Electron range in water

The ranges of electrons in water have been tabulated by M.J. Berger. Values for all energies are found by using the standard linear interpolation method. Table 4.7 shows the values that are used for this linear interpolation.

Table 4.7: Values of electron range in water for different energies. [82]

Energy [MeV]	Range [g cm^{-2}]	Energy [MeV]	Range [g cm^{-2}]
0	0	1	4.367E-1
0.01	2.515E-4	1.5	7.075E-1
0.015	5.147E-4	2	9.785E-1
0.02	8.566E-4	3	1.514
0.03	1.756E-3	4	2.037
0.04	2.919E-3	5	2.55
0.05	4.32E-3	6	3.052
0.06	5.94E-3	8	4.03
0.08	9.77E-3	10	4.975
0.1	1.431E-2	15	7.219
0.15	2.817E-2	20	9.32
0.2	4.487E-2	30	1.317E1
0.3	8.421E-2	40	1.665E1
0.4	1.288E-1	50	1.983E1
0.5	1.766E-1	60	2.276E1
0.6	2.265E-1	80	2.799E1
0.8	3.302E-1	100	3.258E1

Dimensionless dose in water

The previously discussed dimensionless dose in water factors, as listed by Cross, depend on two factors. [81] On the one hand, the equivalent dose will depend on the distance from the source, r, relative to the range of the electron in the medium it travels, r_E. On the other hand, there is also a dependence on energy, E. Cross has listed the factors $j(r/r_E, E)$ for different values of r/r_E and E. Therefore, the method of bilinear interpolation was used for this factor. Table A.1 in appendix A lists the values of $j(r/r_E, E)$ that were used for this interpolation.

4.3.3 Q values of Tb

^{149}Tb, ^{152}Tb and ^{155}Tb are being produced at CERN-MEDICIS.[1] For the future it is expected that a proton beam with a maximum energy of 2.0 GeV and a maximum current of 6 μA will be available for the production of the isotopes. Their expected theoretical maximum activity from this production method is found in table 4.8. [3] While these tabulated values are theoretical predictions, the aim at CERN-MEDICIS is to ship the three Tb isotopes with an activity of 1E-3 TBq. ^{161}Tb is produced in reactor BR2 at SCK•CEN. The final aim is to transport this isotope with an activity of 8 TBq. [87]

[1] For an overview of the production methodology, see [86].

Table 4.8: Expected theoretical maximum activities of the Tb produced at CERN-MEDICIS with a proton beam of energy 2.0 GeV and current 6 μA.

Isotope	Expected Activity [TBq]
^{149}Tb	2.4E-2
^{152}Tb	2.2E-2
^{155}Tb	6.8E-4
^{161}Tb	5.4E-6

At the moment of writing the Q values, and subsequently the A_1 and A_2 values, have only been calculated for ^{149}Tb and ^{161}Tb. [67] This means that ^{152}Tb and ^{155}Tb are subject to the conservative limits from table 3.4. Table 4.9 gives a summary of the current A_1 and A_2 values of all four Tb isotopes.

Table 4.9: Current activity limits for transportation of the Tb isotopes.

Isotope	A_1 [TBq]	A_2 [TBq]
^{149}Tb	8E-1	8E-1
^{152}Tb	1E-1	2E-2
^{155}Tb	1E-1	2E-2
^{161}Tb	3E1	7E-1

It can be seen that the expected theoretical maximum produced activity of ^{152}Tb exceeds its current A_2 value. The produced activity of ^{155}Tb, however, remains below its limits. Nonetheless, with the future in mind, Q values for all four isotopes are calculated. The results for ^{149}Tb and ^{161}Tb can then serve as a reference, to check the validity of the calculation.

The results of the calculations, using the methodologies described in this work, are found in table 4.10. They are compared to values calculated with the System for calculating Exemption and A_1 and A_2 Limits (SEAL) program which are found in table 4.11[2]. [88] The inhalation coefficient of ^{152}Tb is not listed in ICRP 68 nor in IAEA BSS 1996, therefore SEAL was not able to calculate the Q_C value for this isotope. The Q_C value of ^{152}Tb in table 4.10 was calculated with the inhalation coefficient from reference [89].

Table 4.10: Q values for the four Tb isotopes calculated with the methodologies provided in this work.

Isotope	Q_A [TBq]	Q_B [TBq]	Q_C [TBq]	Q_D [TBq]	A_1 [TBq]	A_2 [TBq]
^{149}Tb	7.6E-1	5.5E1	1.2E1	4.4E0	8E-1	8E-1
^{152}Tb	8.0E-1	4.9E0	1.6E2	4.9E0	8E-1	8E-1
^{155}Tb	5.2E0	1.0E3	2.4E2	5.3E0	5E0	5E0
^{161}Tb	2.7E1	3.6E2	4.2E1	6.5E-1	3E1	7E-1

[2]Special thanks to Tiberio Cabianca and Iain Brown for providing me with those values.

Table 4.11: Q values for the four Tb isotopes calculated with SEAL.

Isotope	Q_A [TBq]	Q_B [TBq]	Q_C [TBq]	Q_D [TBq]	A_1 [TBq]	A_2 [TBq]
^{149}Tb	8.2E-1	5.0E1	1.2E1	2.2E0	8E-1	8E-1
^{152}Tb	7.6E-1	5.9E0	-	2.2E0	8E-1	8E-1
^{155}Tb	6.0E0	1.0E3	2.4E2	4.1E0	6E0	4E0
^{161}Tb	2.5E1	2.4E2	4.2E1	7.4E-1	3E1	7E-1

The A_1 and A_2 values have been determined by taking the lowest of the appropriate Q values and rounding it to one significant digit, following the IAEA rules. First note that, although not specifically listed, Q_F has to be determined for ^{149}Tb and ^{152}Tb, since they are alpha-emitters. However, since $Q_F = 10^4 Q_C$, it is immediately clear that Q_F will not influence the A_1 and A_2 values.

Some small numerical differences are found in the Q values when comparing the two different calculation methods. This is to be expected, given the large amount of approximations, interpolations, and different sources that have been used to calculate the values. The values of Q_B and Q_D differ the most between the two methods. This can be expected, since for every discrete energy of the beta particles listed in ICRP 107, a conversion from the interaction of beta particles with water to the interaction of beta particles with air or skin tissue has to be made. The calculation of Q_A uses well established experimental values that were not based on old Monte Carlo simulations. The Q_C values are exactly the same, because they are calculated using the inhalation coefficient that was taken from ICRP 68. For ^{149}Tb and ^{152}Tb, it is Q_A that determines both the A_1 and A_2 value. Note that both isotopes emit β^+-radiation. This means that the secondary produced annihilation radiation, which is taken into account in the calculation of Q_A, plays an important part in the effective dose received due to photons. For ^{155}Tb Q_A still is the limiting factor for the A_1 value. Since this isotope decays through electron capture, this is expected. However, for the A_2 value it is Q_D that is the limiting factor. This means that if the isotope comes in direct contact with the skin, the Auger electrons contribute more to the dose than the X-rays. This can be attributed to the larger range of photons compared to electrons. The same reasoning holds for the β^--emitter, ^{161}Tb. If the isotope is located at a distance, separated by air, the photons will have the most important contribution, so that Q_A is the limiting factor for A_1. However, when applied directly to the skin, the electron contribution becomes the most important one. That is why Q_D is the limiting factor for A_2.
It should furthermore be noted that the small differences in Q values do not lead to different A_1 and A_2 values for all Tb isotopes, except for ^{155}Tb. The differences for this isotope are very small, but still it is desirable to find a more consistent method to calculate the transport activity limits. This method will be elaborated in the next chapter.

5 | FLUKA Simulations

The calculations of the Q_B and Q_D require a cumbersome transformation of values obtained by Monte Carlo simulations in the 1980's and 1990's. Right now, however, there are more advanced Monte Carlo simulation packages available, which allow the direct simulation of the interaction of electrons in air and in skin tissue, without the need for conversion factors. For this reason, FLUKA, a tool developed at CERN, was used to calculate Q_A, Q_B and Q_D values. First, a general description of FLUKA will be given. After that, the methodology used in the simulation will be explained. Then, the obtained results will be presented and compared to the values calculated in the previous chapter. Finally, the consistency of the Monte Carlo method will be put to the test by making a comparison to other values obtained with Monte Carlo methods.

5.1 The FLUKA tool

FLUKA is a multiple-particle transport code that was developed at CERN. It is able to simulate the transport and the interaction with matter of around 60 types of particles. The particle's energy can vary from 100 eV - 1 keV to thousands of TeV. The user-defined geometries in which they travel can be very complex as well. Furthermore, the geometry can be divided into so-called bins. Each bin is considered to be an indivisible point in the geometry where all measured physical properties are identical. The interactions with matter are simulated with advanced microscopic models as much as possible. At every step conservation laws are enforced and results are compared to existing experimental data to ensure consistency of the simulation. As discussed in section 2.2, the interaction of particles with matter is of a stochastic nature. To incorporate this fact, FLUKA uses the principle of Monte Carlo simulations. The user can define an amount of primaries, which can be interpreted as the amount of particles that are transported. Each primary, however, is transported separately. At each step, the stochastic interaction is simulated through random number generation, with a probability distribution corresponding to the actual physical probability distributions. In each bin a detector can be placed to "score" a desired physical quantity, such as absorbed dose, fluence, equivalent dose, etc. These scored physical quantities can and will be different for different primaries due to the random nature of the interactions. The actual physical quantity in a certain bin is then the average of all the scores quantities for each primary. The standard deviation can then serve as a statistical error on the obtained value. Increasing the amount of primaries will therefore increase the accuracy and precision, but it will, however, increase the computing time as well. [90, 91]
For the actual simulations performed in this work, the program *flair* was used. This software serves as an advanced user interface program for FLUKA. Flair provides the

user with an intuitive set of drop-down menus in which settings can be adjusted for every card. It then automatically converts the user input into FLUKA input. Furthermore, it is also possible to visually represent the user-created geometries, to run FLUKA directly from flair and to display a visual representation of the output. [92]

5.2 Methodology

FLUKA allows to define a radioactive isotope on a certain coordinate in the geometry by selecting the appropriate values for the mass number A and atomic number Z. Furthermore, by adding a RADDECAY card all ionising particles and their yield emitted by a certain isotope are requested from ICRP 107. Each nucleus will then decay at a random time, which is generated from the exponential distribution, consistent with eq. (2.2). The radiation emitted is also selected randomly by checking the relative yields from ICRP 107.

Q_A value

For the simulation of Q_A the appropriate Tb isotopes - ^{149}Tb, ^{152}Tb, ^{155}T,b and ^{161}Tb- are selected as source. Since it is not possible to define a one-dimensional point in FLUKA, the Tb sources are defined as a sphere with a radius of 1 cm. They are put in the centre of the geometry and are surrounded by a sphere with a radius of 1.00 m. This sphere consists of air. The atomic constituents of the air used in this simulation are found in table 5.1. The density used was 0.00120479 g cm^{-3}.

Table 5.1: Atomic constituents of air used in the simulation.

Atom	Fraction [%]
Nitrogen	75.53
Oxygen	23.18
Argon	1.28
Carbon	0.01

The sphere consisting of air is surrounded by a larger sphere with an inner radius of 1.00 m and outer radius of 1.05 m. This sphere consists of human skin as defined by the ICRP. The atomic constituents of skin are found in table 5.2. A so-called USRBIN detector is then used to score the particle fluence[1] $\Phi(\epsilon)$ [cm^{-2}] for a primary with initial energy, ϵ, at every bin. With the help of an AUXSCORE card, it is selected that only the transport and interactions of photons will be scored. Using conversion factors $f(\epsilon)$ from Pellicioni [93] the fluence is converted to the effective dose, E, as follows:

$$E = \int f(\epsilon)\Phi(\epsilon)d\epsilon, \tag{5.1}$$

where in practice, equation (5.1) is approximated by a weighted sum over the energies and yields found in ICRP 107. At a distance of 1 m from the source, the effective whole body dose can then be found from the FLUKA output. The units of the result are pSv/primary.

[1] Amount of particles that intersect a unit area.

Since, by definition of the Becquerel, 1 primary = 1 Bq s, the result is multiplied by a factor $C_{pt} = 3600 \times 10^{-12}$ s ph^{-1} = 3.6E-9 s ph^{-1} to obtain the right units of $\dot{e}_{pt}$ [Sv Bq^{-1} h^{-1}]. Finally, Q_A can then be calculated from eq. (3.1).

Table 5.2: Atomic constituents of skin used in the simulation.

Atom	Fraction [%]
Oxygen	61.90
Carbon	22.83
Hydrogen	10.06
Nitrogen	4.64
Chlorine	0.27
Sulfur	0.16
Potassium	0.085
Phosphor	0.033
Calcium	0.015
Sodium	0.007
Magnesium	0.006
Iron	0.001
Zinc	0.001

$\mathbf{Q}_B$ value

The geometry used for the simulation of the Q_B values is identical to the one used for the Q_A values. Furthermore, the AUXSCORE card that is used to filter out only photons is also capable of filtering out only electrons and positrons. However, conversion factors from Pellicioni used in FLUKA are only tabulated for beta energies equal to or higher than 5 MeV. Since none of the beta energies of the Tb isotopes exceed this value, it is not possible to use the same method as for Q_A. Instead, it is chosen to score the absorbed dose, which is expressed in GeV g^{-1} per primary. It should be noted that

$$1\frac{\text{GeV}}{\text{g}} = 1.602176487 \times 10^{-7}\frac{\text{J}}{\text{kg}}. \tag{5.2}$$

Furthermore, 1 J kg^{-1} = 1 Gy. From table 2.1 it can be seen that $w_R = 1$ for beta particles, so that the absorbed dose equals the equivalent dose. Taking into account the conversion from seconds to hours, the results from FLUKA has to be multiplied by a constant C_β = 5.76784E-4 s h^{-1} to obtain $\dot{e}_\beta$ [Sv Bq^{-1} h^{-1}]. After that eq. (3.3) is used to find Q_B.

$\mathbf{Q}_D$ value

Since Q_D is computed completely different from Q_A and Q_B, a different geometry is used. To start with, the Tb source is now a three-dimensional object itself; it is a cuboid with a surface of 1 cm^2 and a thickness of 1 μm.[2] The Tb source is placed on the centre of

[2]This is an arbitrary choice of thickness, since it is found that the thickness did not influence the result.

one side of a 100 cm^3 cube, that consists of skin material as specified in table 5.2. Again, AUXSCORE is used to filter out only the beta particles. Since the beta particles do not reach the threshold of 5 MeV, the same methodology as for Q_B is used to obtain the equivalent dose. Since the equivalent skin dose rate, $\dot{h}$, is expressed in inverse seconds instead of inverse hours, it is not necessary to add the extra factor of 3600. It is however necessary to add an extra factor of 10^{-4} to convert cm^2 to m^2, so that the FLUKA results need to be multiplied with a factor C_h = 1.602176487E-2 s h^{-1} to obtain the right units for $\dot{h}$ [Sv m^2 Bq^{-1} s^{-1}]. Q_D can then be calculated with eq. (3.7).

5.3 Simulation results of Tb isotopes

Figure 5.1(a) gives an example of a simulation used to find the photon dose rate, $\dot{e}_{pt}$, for ^{149}Tb. All other plots are found in appendix B. The Tb source is found at the centre of the coordinate system $(x, y) = (0, 0)$. The black circle is also centred at this coordinate and has a radius of 100 cm. Therefore, it represents the distance of 100 cm between the source and the exposed worker. The material within the circle is air, while outside of the circle it is skin tissue. Figure 5.1(b) focuses on the region were the value of $\dot{e}_{pt}$ have been measured along with its statistical error. Again, the black line indicates the interface between the air and skin tissue. The results of this are found in table 5.3.

An example for the simulation of the equivalent skin dose rate, $\dot{e}_{\beta}$, for ^{149}Tb is found in figure 5.2(a). The other plots are found in appendix B. Again, the Tb source is located at $(x, y) = (0, 0)$ and the black circle represents the distance of 100 cm from the source. Notice that, in contrast with the simulation of $\dot{e}_{pt}$, the equivalent dose rate quickly drops to zero after the beta particles enter the skin tissue. This can be attributed to the fact that beta particles are much more easily stopped compared to photons as explained in chapter 2. Figure 5.2(b) again focuses on the region were $\dot{e}_{\beta}$ was measured. The FLUKA results of $\dot{e}_{\beta}$ along with their statistical errors for all Tb isotopes are found in table 5.3.

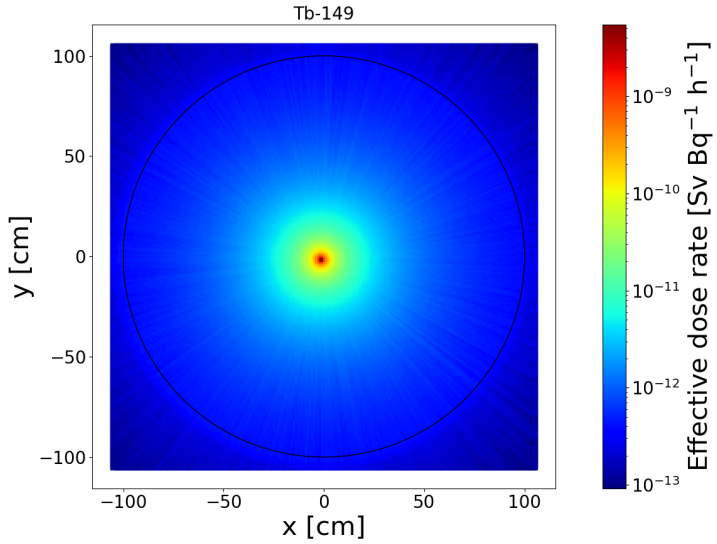

(a) 2D plot of the FLUKA simulation for the effective dose rate of ^{149}Tb to calculate Q_A. The source is located at the centre of the plot. The black circle indicates the radius of 1.00 m, which is the interface between air and skin tissue.

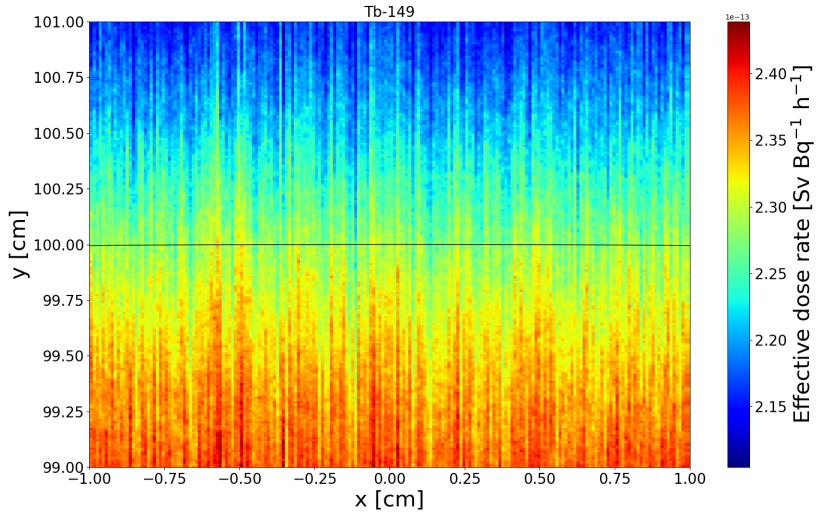

(b) Zoomed in version of the 2D plot of the FLUKA simulation for the effective dose rate of ^{149}Tb to calculate Q_A. The black line indicates the location on which the effective dose rate was scored.

Figure 5.1: 2D plot of the FLUKA simulation for the effective dose rate of ^{149}Tb to calculate Q_A.

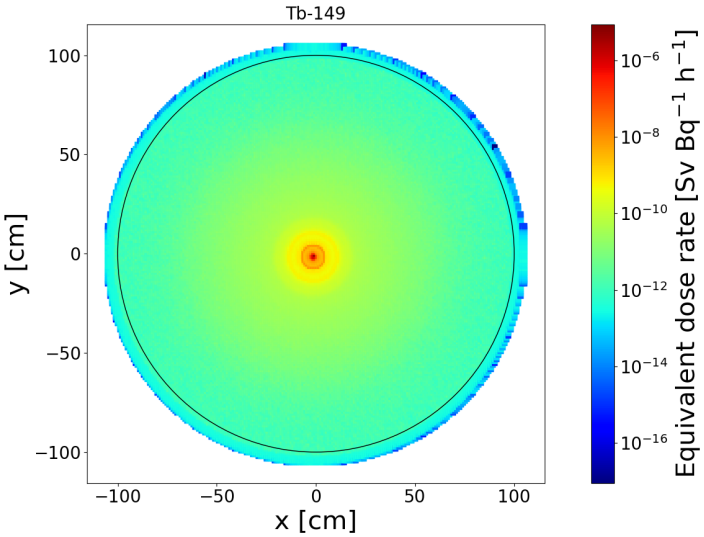

(a) 2D plot of the FLUKA simulation for the equivalent skin dose rate of ^{149}Tb to calculate Q_B. The source is located at the centre of the plot. The black circle indicates the radius of 1.00 m, which is the interface between air and skin tissue.

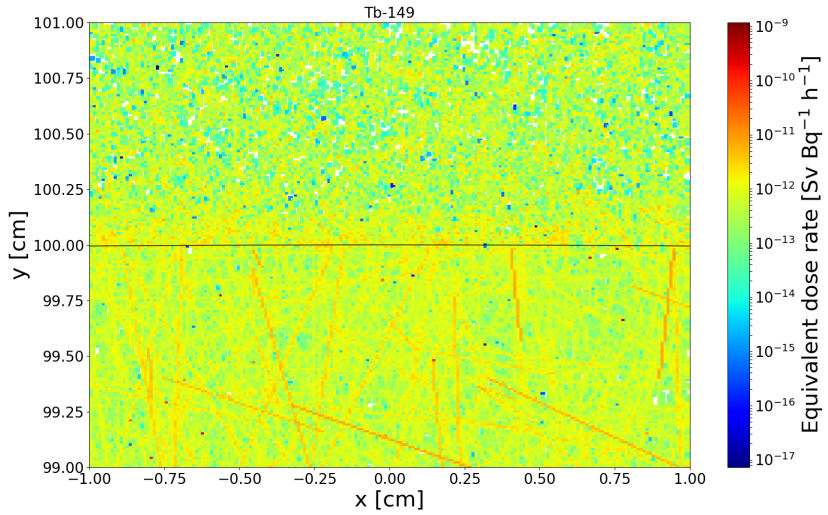

(b) Zoomed in version of the 2D plot of the FLUKA simulation for the equivalent skin dose rate of ^{149}Tb to calculate Q_B. The black line indicates the location on which the equivalent skin dose rate was scored.

Figure 5.2: 2D plot of the FLUKA simulation for the equivalent skin dose rate of ^{149}Tb to calculate Q_B.

Finally, a plot of the simulation for the equivalent skin dose rate, $\dot{h}$, for ^{149}Tb is found in figure 5.3(a). The plane Tb source extends from y = -0.5 cm to y = 0.5 cm at x = -5 cm. The region on the right hand side of the source consists of skin tissue, while the region on the left hand side consists of air. Figure 5.3(b) zooms in to a skin depth varying from 50 μm to 90 μm. The plane Tb source is not visible on this plot. Nonetheless, the red bar in the centre of the plot clearly indicates the region of the skin that is located below the source. Since x-axis marks the centre of the terbium source, the equivalent skin dose

rate was scored on the x-axis at a skin depth of 70 μm. The results for all Tb isotopes are found in table 5.3.

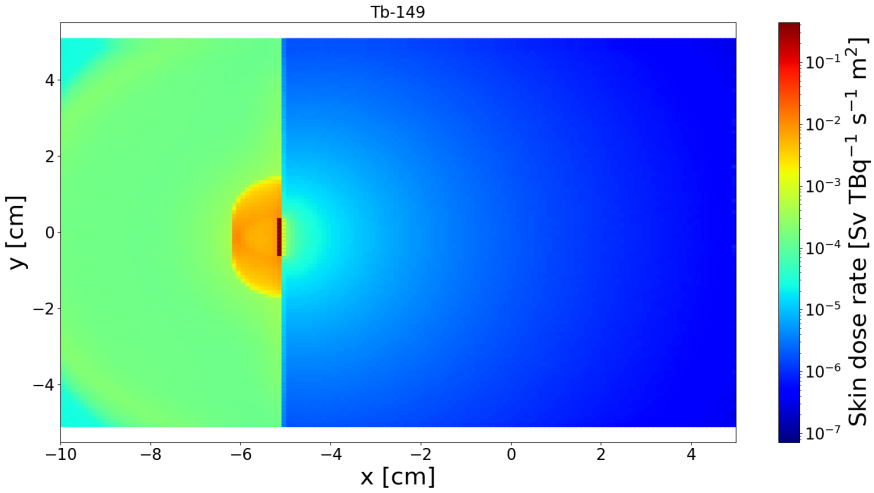

(a) 2D plot of the FLUKA simulation for the equivalent skin dose rate of ^{149}Tb to calculate Q_D. The Tb source extends from y = -0.5 cm to y = 0.5cm at x = -5 cm. The right hand side of the source consists of skin tissue, while the life hand side consists of air.

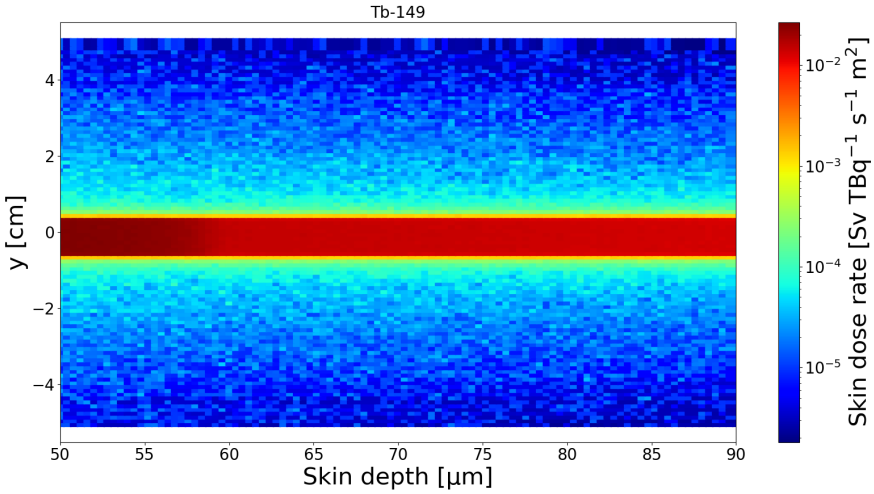

(b) Zoomed in version of the 2D plot of the FLUKA simulation for the equivalent skin dose rate of ^{149}Tb to calculate Q_D.

Figure 5.3: 2D plot of the FLUKA simulation for the equivalent skin dose rate of ^{149}Tb to calculate Q_B.

Table 5.3: FLUKA simulation results for the effective dose rates and equivalent skin dose rates used for the calculation of Q_A, Q_B and Q_D. (Statistical error between brackets.)

Isotope	$\dot{e}_{pt}$ $[\frac{\text{Sv}}{\text{Bq h}}]$	$\dot{e}_{\beta}$ $[\frac{\text{Sv}}{\text{Bq h}}]$	$\dot{h}$ $[\frac{\text{Sv m}^2}{\text{TBq s}}]$
^{149}Tb	2.3E-13 (0.81 %)	4.6E-13 (3.92 %)	1.5E-2 (1.14 %)
^{152}Tb	2.8E-13 (1.19 %)	9.7E-13 (6.04 %)	9.8E-3 (0.69 %)
^{155}Tb	6.7E-14 (1.19 %)	5.0E-14 (5.66 %)	2.9E-3 (3.46 %)
^{161}Tb	1.4E-14 (3.58 %)	1.7E-14 (5.2 %)	2.9E-2 (1.00 %)

The statistical error of the $\dot{e}_{\beta}$ values is noticeably higher than that of the other Q values. This can be attributed to the fact that beta particles are more easily stopped, so that fewer particles will reach the region in which the dose rate is scored, when using the same number of primaries.
Combining the values from table 5.3 with the values of Q_C, which are calculated in the previous chapter, a new set of Q values for the Tb isotopes is found. From this a new set of A_1 and A_2 values is obtained. The newly obtained Q values and activity limits are compared with those obtained through the numerical methods, which were discussed in the previous chapter, in table 5.4.

Table 5.4: The Q values and A_1 and A_2 values for the Tb isotopes obtained with FLUKA compared to the numerically obtained values.

Isotope	Method	Q_A [TBq]	Q_B [TBq]	Q_C [TBq]	Q_D [TBq]	A_1 [TBq]	A_2 TBq
^{149}Tb	FLUKA	4.3E-1	2.2E0	1.2E1	1.9E0	4E-1	4E-1
	Own numerical	7.6E-1	5.5E1	1.2E1	4.4E0	8E-1	8E-1
	SEAL	8.2E-1	5.0E1	1.2E1	2.2E0	8E-1	8E-1
^{152}Tb	FLUKA	3.5E-1	1.0E0	1.6E2	2.9E0	4E-1	4E-1
	Own numerical	8.0E-1	4.9E0	1.6E2	4.9E0	8E-1	8E-1
	SEAL	7.6E-1	5.9E0	-	2.2E0	8E-1	8E-1
^{155}Tb	FLUKA	1.5E0	2.0E1	2.4E2	9.8E0	2E0	2E0
	Own numerical	5.2E0	1.0E3	2.4E2	5.3E0	5E0	5E0
	SEAL	60.E0	1.0E3	2.4E2	4.1E0	6E0	4E0
^{161}Tb	FLUKA	7.2E0	5.9E1	4.2E1	9.7E-1	7E0	1E0
	Own numerical	2.7E1	3.6E2	4.2E1	6.5E-1	3E1	7E-1
	SEAL	2.5E1	2.4E2	4.2E1	7.4E-1	3E1	7E-1

A comparison is made between these values and the numerical values obtained by calculations performed in this work (table 4.10) or performed by SEAL (table 4.11). Some noticeable differences can be observed. A first observation is that the Monte Carlo method consistently leads to more conservative Q values. The limiting factors, however, remain the same for all four isotopes. For ^{149}Tb, ^{152}Tb and ^{161}Tb, Q_A remains the limiting value for both A_1 and A_2. For ^{161}Tb, Q_A remains the limiting factor for A_1, while Q_D determines A_2. When comparing the Q_A values, the values remain approximately in the same order of magnitude. However, when looking at Q_B and Q_D values, some very large

differences are observed. The most notable being the Q_B values of ^{149}Tb and ^{152}Tb and the Q_D values of ^{152}Tb and ^{155}Tb. This suggests that some ad hoc assumptions made in the numerical method, might lead to a serious underestimation of the equivalent dose. In general, FLUKA leads to more conservative A_1 and A_2 values for all isotopes. Since it is unclear at this point, which method will lead to the most consistent results, the Monte Carlo values obtained in this work should be compared to other values obtained with a Monte Carlo method. This is discussed in the next section.

5.4 Comparison of Q values calculated with Monte Carlo simulations

FLUKA has been used in the past as a means of calculating Q_B and Q_D values by P. Bertreix and T. Frosio. [94] They have calculated those values for various isotopes produced at CERN-MEDICIS, including ^{149}Tb and ^{152}Tb. In the previous chapter is has been shown that the numerical methods could lead to notable differences in the Q values calculated by two independent parties. This is mostly attributable to the fact that the IAEA leave much room for interpretation. The choice of source material and interpolation methods used for tabulated values is left to the person who calculates the Q values. To check whether Monte Carlo simulations lead to more consistent results, a comparison with the results from P. Bertreix and T. Frosio is made. The same methodologies as for the four Tb isotopes is used. P. Bertreix and T. Frosio reported a statistical error below 0.8 % for all values. [94] The comparison is found in table 5.5.

Table 5.5: Comparison of the results for Q_B with the values from P. Bertreix and T. Frosio. [94]

	Q_B [TBQ]		
Isotope	Bertreix & Frosio	This work	Error (this work)[%]
^{61}Cu	1.2E0	1.2E0	3.32
^{71}As	1.2E1	1.3E1	2.12
^{140}Nd	4.3E-1	4.6E-1	3.59
^{149}Tb	2.7E0	2.2E0	3.92
^{152}Tb	1.0E0	1.0E0	6.04
^{166}Yb	5.0E0	5.4E0	3.11
^{213}Bi	5.1E-1	4.7E-1	1.82

At first glance, the results seem to agree better than the numerical results. Small differences are still found in the two different methods. They can be attributed to the fact that Monte Carlo simulation never lead to the exact same results, due to the random nature of this method. Furthermore, the fact that the considered doses are extremely low, can also contribute to inaccuracies. Finally, every body defined in FLUKA is a three-dimensional object. While IAEA requires point sources to be used, these point sources have to be approximated with a very small sphere, or cube, or cylinder, etc. Since, IAEA does not specify which option should be used, it is again a choice of the person who performs the simulation. This means that two Monte Carlo methods can both be conform to the

transport regulations, but still lead to small numerical differences. Nonetheless, in the previous chapter a relative difference of 50 % was found between the two Q_B values of ^{161}Tb. The largest difference in the Q_B values calculated with FLUKA is 18.5 % for ^{149}Tb. This is still larger than any of the statistical errors mentioned, due to the reasons mentioned earlier. This shows that Monte Carlo simulations can lead to more consistent results. However, care should still be taken to draw final conclusions, since only a small amount of results is available for comparison.

To illustrate that changing the dimensions of the radioactive source in the simulation can lead to different numerical results, $\dot{e}_\beta$ and Q_B are calculated with a spherical Tb source with a radius of 0.0001 cm instead of a radius of 1 cm. The other simulation conditions are left unchanged. The results are found in table 5.6. Here it can be seen that changing geometry conditions lead to numerical differences up to 20 % in the case of ^{152}Tb. This is much larger than the statistical error on the Q_B value of ^{152}Tb, which is 6.04 %.

Table 5.6: The results of the Q_B values for the Tb isotopes using a 1 cm spherical source compared to a 0.0001 cm spherical source.

Isotope	Source radius [cm]	$\dot{e}_\beta$ [$\frac{\text{Sv}}{\text{Bq h}}$]	Q_B [TBq]
^{149}Tb	1	4.6E-13	2.2E0
	1E-4	4.3E-13	2.3E0
^{152}Tb	1	9.7E-13	1.0E0
	1E-4	8.0E-13	1.2E0
^{155}Tb	1	5.0E-14	2.0E1
	1E-4	5.1E-14	2.0E1
^{161}Tb	1	1.7E-14	5.9E1
	1E-4	1.6E-14	6.3E1

In table 5.7 the comparison for Q_D values can be found. P. Bertreix and T. Frosio reported a maximum statistical error of 0.3 % on their values. [94]

Table 5.7: Comparison of the results for Q_D with the values from P. Bertreix and T. Frosio.

	Q_D [TBQ]		
Isotope	Bertreix & Frosio	This work	Error (this work) [%]
^{61}Cu	9.5E-1	1.0E0	0.47
^{71}As	1.5E0	1.6E0	0.28
^{140}Nd	1.2E0	1.3E0	0.15
^{149}Tb	2.3E0	1.9E0	1.14
^{152}Tb	2.8E0	2.9E0	0.69
^{166}Yb	6.0E-1	6.5E-1	2.03
^{213}Bi	3.2E-1	3.8E-1	1.30

Again, there is a better agreement between the Q_D values compared to the numerical method. The largest relative difference is 123 % for ^{152}Tb in the previous chapter. The largest relative difference for the Monte Carlo methods is 19 % for ^{213}Bi. The fact that there are still some differences for the Q_D mostly has the same reasons as those described for Q_B. Furthermore, Q_D values are calculated from doses at a depth of 70 μm. This distance is very small compared to other dimensions used in the simulation. The source, for example, has a surface of 1 cm^2. In general, the Monte Carlo method appears to be more consistent than the numerical method for Q_D values. Again, it should be noted that only a limited amount of other results is available, so that conclusions should be made with caution.

5.5 Proposed A_1- and A_2 values

The results obtained with FLUKA lead to the most consistent results for every Q value calculated in this work. Furthermore, the FLUKA results always lead to more conservative Q values. Keeping in mind that the IAEA is also investigating Monte Carlo methods to replace the old numerical methods for the Q system, the final A_1 and A_2 values for the four Tb isotopes are chosen to be the ones obtained with FLUKA in this work. The A_1 and A_2 values of the four Tb isotopes, that are calculated with FLUKA, are found in 5.8. For ^{149}Tb and ^{161}Tb, the activity limits are lower than the ones currently listed in IAEA SSR-6. [67] For ^{152}Tb and ^{155}Tb the limits have not been determined yet, so the tabulated values are the ones that are proposed.

Table 5.8: Comparison of the simulated A_1 and A_2 values for ^{149}Tb and ^{161}Tb with their respective IAEA limits. Proposed A_1 and A_2 values for ^{152}Tb and ^{155}Tb.

Isotope	Method	A_1 [TBq]	A_2 TBq
^{149}Tb	Own	4E-1	4E-1
	IAEA	8E-1	8E-1
^{152}Tb	Own	4E-1	4E-1
	IAEA	-	-
^{155}Tb	Own	2E0	2E0
	IAEA	-	-
^{161}Tb	Own	7E0	1E0
	IAEA	3E1	7E-1

6 | Conclusion and Outlook

In this work the regulations on the transport of radioactive material are investigated. The main goal is to be able to transport four terbium isotopes - ^{149}Tb, ^{152}Tb, ^{155}Tb and ^{161}Tb - in Type A packages. The first part consists of a literature study on national and international regulatory bodies and their functions. The main focus is on the transport regulations, formed by the IAEA. It is found that, in order for isotopes to be allowed to be transported in Type A packages, their activity has to be below the predetermined A_1 and A_2 values. These values can be calculated using the Q system that is worked out by the IAEA. The Q system, as it stands now, requires the calculation of five Q values that represent five different pathways for radiation exposure. The IAEA defines each Q value and gives basic guidelines on how to calculate them, based on ad hoc assumptions. Furthermore, there are not always guidelines on which source material should be consulted for physical values, as well as interpolation methods that need to be used for tabulated values. This work shows that this leads to discrepancies between two independently calculated Q values of the same Tb isotope. While there are numerical differences, after rounding values, the two methods agree on A_1 and A_2 values for all Tb isotopes, except ^{155}Tb. Even for this isotope the difference is minimal.

In the second part of this work, Monte Carlo methods are investigated. The goal is to find a more consistent method of calculating Q values. The Monte Carlo tool used for this purpose is FLUKA. This tool allows to calculate effective doses and equivalent doses for different isotopes. The first simulations for the four Tb isotopes lead, consistently, to more conservative values than those calculated numerically. When comparing the Monte Carlo method with the numerical method, it is found that Q_A values are reproduced with the same order of magnitude. The values of Q_B and Q_D, however, show some very large differences. Nonetheless, the limiting Q values for the A_1 and A_2 values remain the same, although they differ in numerical values.

To find the most consistent method of calculating Q values, FLUKA was also used to calculate Q_B and Q_D values for various isotopes produced at CERN-MEDICIS. These values have been calculated earlier with FLUKA by P. Bertreix and T. Frosio, so that they can be compared to the values calculated in this work. It is found that the Monte Carlo method indeed leads to much more consistent results for all isotopes that are considered. Care should be taken, however, since the sample of available isotopes to test the consistency of Monte Carlo methods is not very large. Furthermore, it remains unclear how much of the numerical differences in the values of the Monte Carlo method can be attributed to different choices of geometry in the simulation itself.

Right now, IAEA is also investigating the possibility of implementing Monte Carlo methods in the Q system. Their motivation is the fact that the current Q system is based on ad hoc assumptions and that some calculation methods are left open for interpretation. To make the calculation of Q values more scientifically rigorous, and to make results more consistent, different Monte Carlo programs are being tested.

Since the results of this work indicate that the Monte Carlo method gives the most reliable Q values, the proposed A_1 and A_2 values for ^{152}Tb and ^{155}Tb will be based on this method. For ^{152}Tb the A_1 and A_2 values both are suggested to be 4E-1 TBq. For ^{155}Tb the A_1- and A_2 values both are suggested to be 2E0 TBq.

Appendices

A | Table of dimensionless dose constants from Cross

Table A.1: Values of $j(r/r_E, E)$ for different ranges and energies. [81]

Energy [MeV] / r/r_E	0.025	0.05	0.1	0.2	0.4	0.7	1	2	4
0	0.564	0.57	0.589	0.627	0.692	0.761	0.807	0.892	0.952
0.025	0.58	0.587	0.6	0.642	0.7	0.773	0.814	0.902	0.96
0.05	0.599	0.604	0.613	0.658	0.714	0.787	0.821	0.91	0.965
0.075	0.62	0.623	0.632	0.676	0.732	0.8	0.833	0.92	0.972
0.1	0.643	0.645	0.656	0.697	0.751	0.816	0.847	0.93	0.978
0.125	0.67	0.67	0.683	0.718	0.772	0.832	0.862	0.939	0.985
0.15	0.703	0.701	0.712	0.744	0.797	0.847	0.877	0.95	0.992
0.175	0.74	0.734	0.744	0.768	0.819	0.864	0.894	0.961	0.998
0.2	0.78	0.767	0.777	0.801	0.844	0.885	0.914	0.974	1.005
0.225	0.824	0.805	0.815	0.832	0.872	0.907	0.935	0.988	1.012
0.25	0.87	0.853	0.861	0.872	0.905	0.936	0.956	1.003	1.018
0.275	0.921	0.9	0.906	0.917	0.942	0.964	0.979	1.02	1.027
0.3	0.98	0.952	0.957	0.966	0.984	0.998	1.01	1.04	1.036
0.325	1.043	1.005	1.007	1.2	1.031	1.038	1.046	1.057	1.048
0.35	1.107	1.068	1.068	1.077	1.088	1.087	1.085	1.082	1.063
0.375	1.175	1.138	1.134	1.138	1.149	1.14	1.135	1.113	1.079
0.4	1.251	1.212	1.202	1.207	1.21	1.195	1.193	1.148	1.096
0.425	1.329	1.289	1.271	1.278	1.273	1.251	1.252	1.185	1.115
0.45	1.403	1.373	1.342	1.348	1.341	1.308	1.308	1.221	1.141
0.475	1.471	1.453	1.411	1.416	1.407	1.365	1.36	1.259	1.17
0.5	1.53	1.517	1.478	1.481	1.468	1.423	1.405	1.299	1.198
0.525	1.578	1.569	1.54	1.541	1.52	1.477	1.444	1.34	1.226
0.55	1.612	1.612	1.594	1.596	1.561	1.523	1.481	1.383	1.252
0.575	1.632	1.642	1.635	1.64	1.59	1.557	1.507	1.419	1.275
0.6	1.639	1.661	1.662	1.667	1.606	1.574	0.514	1.436	1.295
0.625	1.625	1.659	1.668	0.67	1.606	1.571	1.507	1.437	1.307
0.65	1.578	1.625	1.641	1.638	1.587	1.544	1.489	1.42	1.308
0.675	1.505	1.565	1.588	1.578	1.542	1.497	1.453	1.387	1.297
0.7	1.404	1.483	1.516	1.489	1.461	1.434	1.396	1.28	1.236
0.725	1.289	1.378	1.42	1.379	0.1355	1.348	1.316	1.28	1.236
0.75	1.173	1.246	1.291	1.257	1.232	1.226	1.206	1.175	1.166
0.775	1.05	1.102	1.143	1.119	1.093	1.083	1.075	1.05	1.077
0.8	0.916	0.958	0.984	0.959	0.94	0.931	0.924	0.92	0.974
0.825	0.78	0.812	0.82	0.792	0.78	0.771	0.764	0.784	0.857
0.85	0.648	0.661	0.66	0.629	0.615	0.599	0.605	0.642	0.723
0.875	0.523	0.518	0.51	0.477	0.457	0.438	0.455	0.499	0.583
0.9	0.409	0.398	0.377	0.45	0.32	0.312	0.324	0.358	0.443
0.925	0.308	0.296	0.263	0.235	0.207	0.21	0.213	0.233	0.313
0.95	0.227	0.211	0.176	0.155	0.128	0.128	0.128	0.142	0.205
0.975	0.162	0.144	0.111	0.096	0.074	0.068	0.067	0.077	0.12
1	0.114	0.094	0.066	0.053	0.039	0.034	0.034	0.038	0.066
1.025	0.079	0.059	0.036	0.024	0.019	0.016	0.017	0.016	0.032
1.05	0.054	0.035	0.019	0.009	0.009	0.008	0.009	0.006	0.014
1.075	0.035	0.02	0.01	0.005	0.003	0.002	0.002	0.002	0.005
1.1	0.02	0.011	0.005	0.003	0	0	0	0.001	0.004
1.125	0.004	0.005	0.002	0.001	0	0	0	0.001	0.002
1.15	0	0	0	0	0	0	0	0	0

B | FLUKA plots

B.1 Q_A value

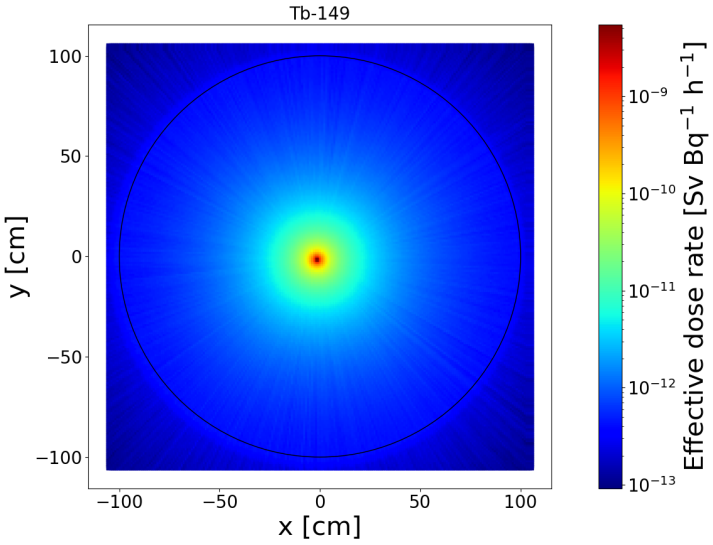

Figure B.1: Effective dose rate for ^{149}Tb

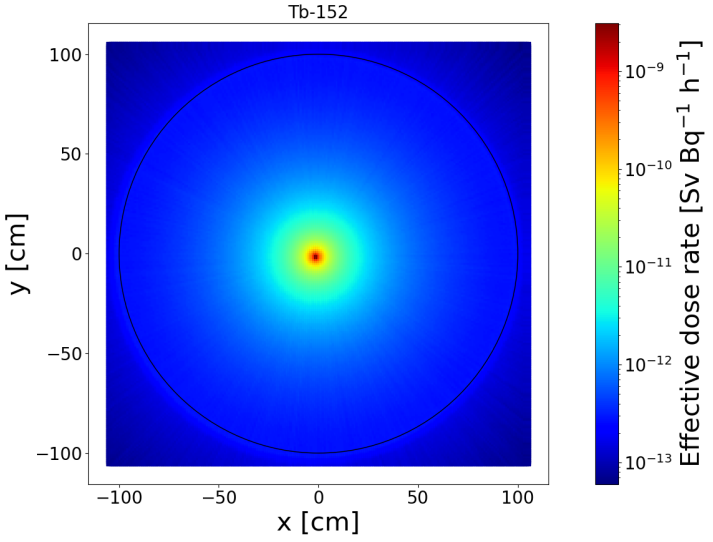

Figure B.2: Effective dose rate for ^{152}Tb

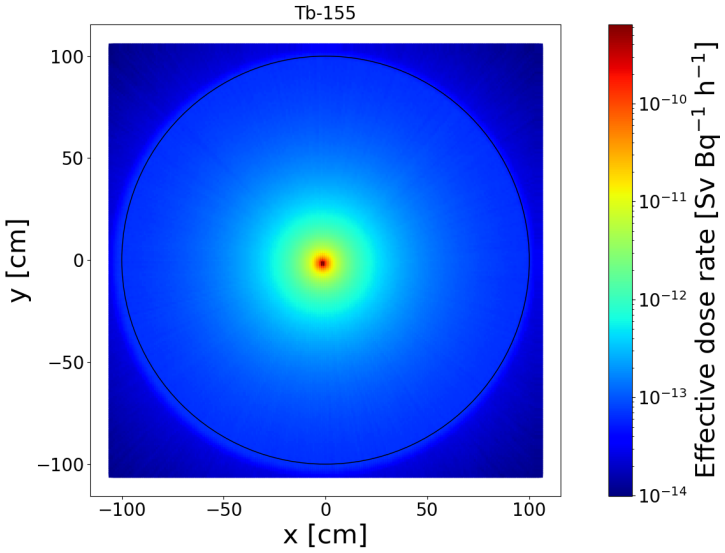

Figure B.3: Effective dose rate for ^{155}Tb

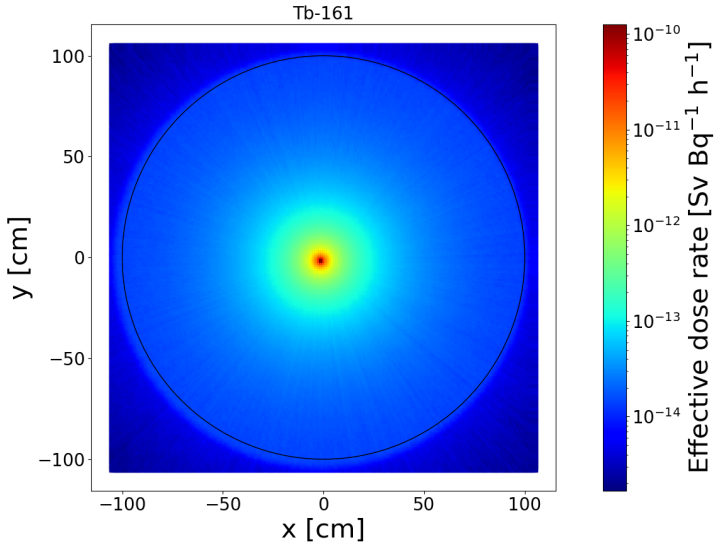

Figure B.4: Effective dose rate for ^{161}Tb

B.2 Q_B value

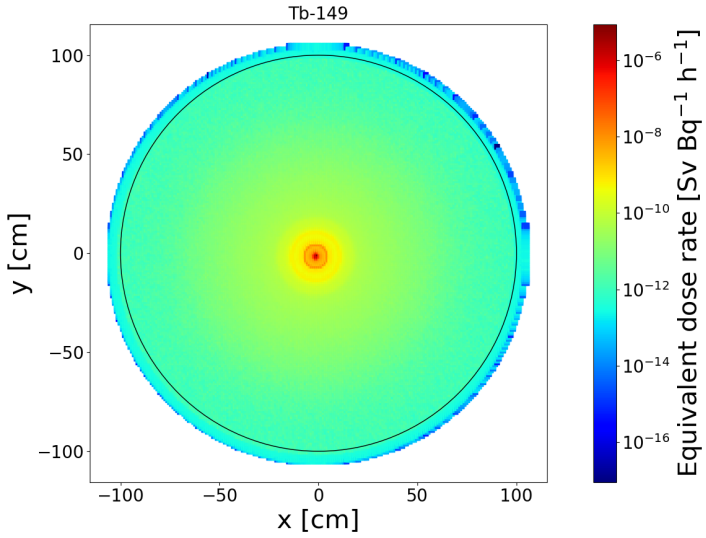

Figure B.5: Equivalent dose rate for ^{149}Tb

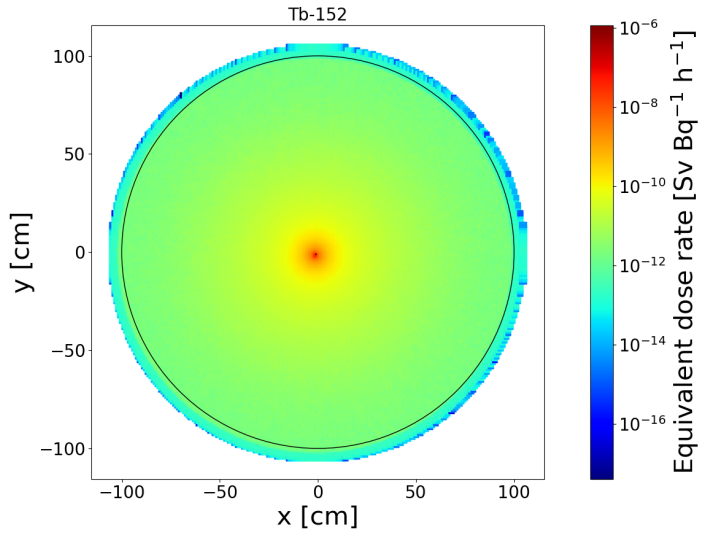

Figure B.6: Equivalent dose rate for ^{152}Tb

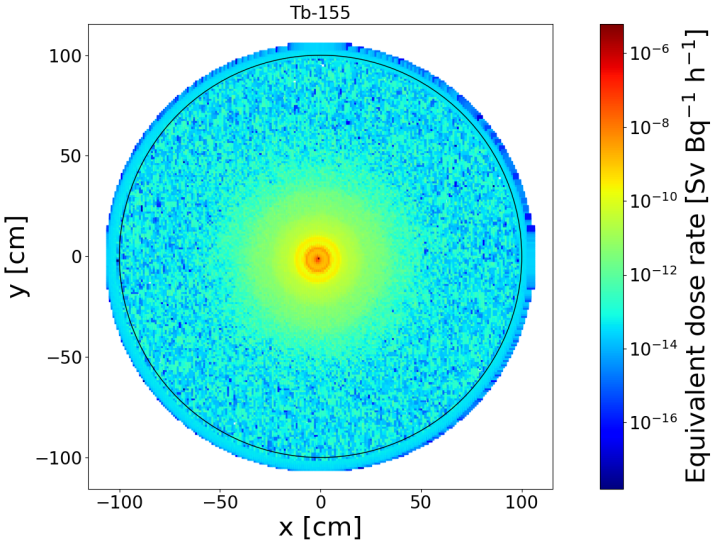

Figure B.7: Equivalent dose rate for ^{155}Tb

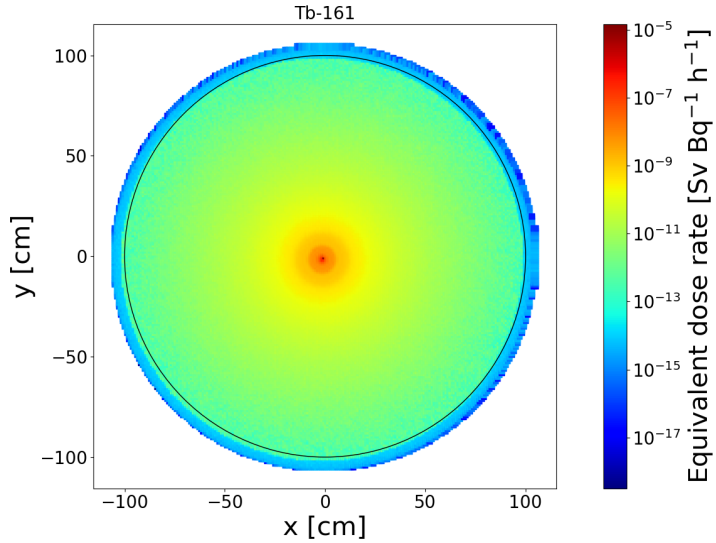

Figure B.8: Equivalent dose rate for ^{161}Tb

B.3 Q_D value

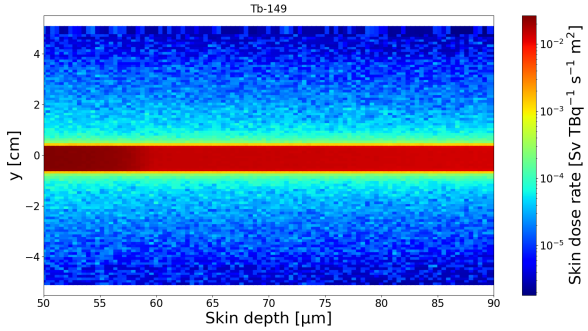

Figure B.9: Equivalent skin dose rate for ^{149}Tb

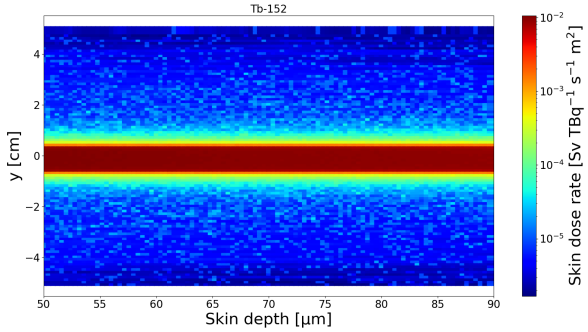

Figure B.10: Equivalent skin dose rate for ^{152}Tb

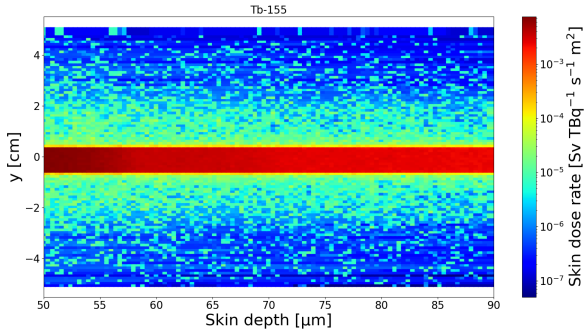

Figure B.11: Equivalent skin dose rate for ^{155}Tb

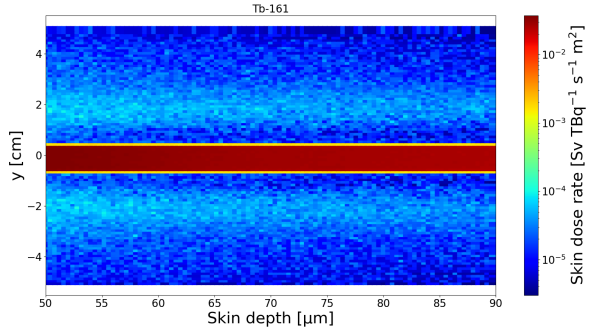

Figure B.12: Equivalent skin dose rate for ^{161}Tb

Bibliography

[1] E. O. Lawrence and N. E. Edlefsen, "On the production of high speed protons," *Science*, vol. 72, no. 1867, p. 376, 1930.

[2] J. E. Williams, "Donner laboratory: The birthplace of nuclear medicine," *Journal of Nuclear Medicine*, vol. 40, no. 1, pp. 16N–20N, 1999.

[3] R. dos Santos Augusto, L. Buehler, Z. Lawson, S. Marzari, M. Stachura, T. Stora, C.-M. collaboration, *et al.*, "Cern-medicis (medical isotopes collected from isolde): a new facility," *Applied Sciences*, vol. 4, no. 2, pp. 265–281, 2014.

[4] https://www.sckcen.be/nl/Research/Infrastructure/BR2. Accessed: 05-06-2019.

[5] K. S. Krane, *Introductory nuclear physics*. John Wiley & Sons, 1988.

[6] "Binding energy curve." http://www.splung.com/content/sid/5/page/benergy. Accessed: 29-01-2019.

[7] J. M. Blatt and V. F. Weisskopf, *Theoretical nuclear physics*. Courier Corporation, 1991.

[8] "Isotope stability." https://chem.libretexts.org/Bookshelves/Physical_and_Theoretical_Chemistry_Textbook_Maps/Supplemental_Modules_(Physical_and_Theoretical_Chemistry)/Nuclear_Chemistry/Nuclear_Energetics_and_Stability/Nuclear_Magic_Numbers. Accessed: 04-02-2019.

[9] R. W. Gurney and E. U. Condon, "Wave mechanics and radioactive disintegration," *Nature*, vol. 122, no. 3073, p. 439, 1928.

[10] H. Mang, "Alpha decay," *Annual Review of Nuclear Science*, vol. 14, no. 1, pp. 1–26, 1964.

[11] W. C. Haxton and B. R. Holstein, "Neutrino physics," *American Journal of Physics*, vol. 68, no. 1, pp. 15–32, 2000.

[12] P. J. Mohr, D. B. Newell, and B. N. Taylor, "Codata recommended values of the fundamental physical constants: 2014," *Rev. Mod. Phys.*, vol. 88, p. 035009, Sep 2016.

[13] L. W. Alvarez, "The capture of orbital electrons by nuclei," *Phys. Rev.*, vol. 54, pp. 486–497, Oct 1938.

[14] F. L. Wilson, "Fermi's theory of beta decay," *American Journal of Physics*, vol. 36, no. 12, pp. 1150–1160, 1968.

[15] M. Bhat, "Evaluated nuclear structure data file (ensdf)," in *Nuclear Data for Science and Technology*, pp. 817–821, Springer, 1992.

[16] D. Finkenthal, B. Greco, R. Halsey, L. Pena, S. Rodecker, B. Simms, R. L. Lee, J. Lohr, M. J. Schaffer, and D. P. Schissel, "Introduction to the electromagnetic spectrum," *General Atomic*, p. 46, 1996.

[17] L. Sodickson, W. Bowman, J. Stephenson, and R. Weinstein, "Single-Quantum Annihilation of Positrons," *Physical Review*, vol. 124, pp. 1851–1861, Dec. 1961.

[18] R. Van Grieken and A. Markowicz, *Handbook of X-ray Spectrometry*. CRC press, 2001.

[19] D. J. Griffiths, "Introduction to electrodynamics," 2005.

[20] P. J. Woods and C. N. Davids, "Nuclei beyond the proton drip-line," *Annual Review of Nuclear and Particle Science*, vol. 47, no. 1, pp. 541–590, 1997.

[21] N. Tralli, "The theory of internal conversion," *Physical Review*, vol. 83, 07 1951.

[22] T. L. Alford, L. C. Feldman, and J. W. Mayer, *Fundamentals of nanoscale film analysis*. Springer Science & Business Media, 2007.

[23] N. Bohr and J. A. Wheeler, "The mechanism of nuclear fission," *Physical Review*, vol. 56, no. 5, p. 426, 1939.

[24] D. R. Lide *et al.*, *CRC handbook of chemistry and physics*. CRC Boca Raton, 2012.

[25] G. F. Knoll, *Radiation detection and measurement*. John Wiley & Sons, 2010.

[26] B. Wilken and T. A. Fritz, "Energy distribution functions of low energy ions in silicon absorbers measured for large relative energy losses," *Nuclear Instruments and Methods*, vol. 138, no. 2, pp. 331–343, 1976.

[27] H. Bethe, "H. bethe, z. phys. 76, 293 (1932).," *Z. Phys.*, vol. 76, p. 293, 1932.

[28] F. Bloch, "Zur bremsung rasch bewegter teilchen beim durchgang durch materie," *Annalen der Physik*, vol. 408, no. 3, pp. 285–320, 1933.

[29] W. H. Bragg and R. Kleeman, "Lxxiv. on the ionization curves of radium," *The London, Edinburgh, and Dublin Philosophical Magazine and Journal of Science*, vol. 8, no. 48, pp. 726–738, 1904.

[30] J. M. Stellman, *Encyclopaedia of occupational health and safety*, vol. 1. International Labour Organization, 1998.

[31] K. Abdullah, *Fundamentals in nuclear physics*. University of Duhok, 12 2014.

[32] R. Bogaert, "Lecture notes in radiation protection," 2017.

[33] A. Einstein, "Über einen die erzeugung und verwandlung des lichtes betreffenden heuristischen gesichtspunkt," *Annalen der physik*, vol. 322, no. 6, pp. 132–148, 1905.

[34] R. Evans, *The atomic nucleus*. McGraw-Hill New York, 1955.

[35] A. H. Compton, "A quantum theory of the scattering of x-rays by light elements," *Physical review*, vol. 21, no. 5, p. 483, 1923.

[36] O. Klein and Y. Nishina, "Über die streuung von strahlung durch freie elektronen nach der neuen relativistischen quantendynamik von dirac," *Zeitschrift für Physik*, vol. 52, no. 11-12, pp. 853–868, 1929.

[37] D. Ashok and F. Thomas, *Introduction to nuclear and particle physics*. World Scientific, 2003.

[38] J. E. Turner, *Atoms, radiation, and radiation protection*. John Wiley & Sons, 2008.

[39] M. G. Stabin, *Radiation protection and dosimetry: an introduction to health physics*. Springer Science & Business Media, 2007.

[40] J. Shapiro, *Radiation protection: a guide for scientists, regulators, and physicians*. La Editorial, UPR, 2002.

[41] https://teachnuclear.ca/all-things-nuclear/radiation/biological-effects-of-radiation/effects-of-ionizing-radiation-on-dna/. Accessed: 31-05-2019.

[42] http://www.bioquicknews.com/node/2696. Accessed: 31-05-2019.

[43] J. Bergonie, "De quelques resultas de la radiotherapie et essai de fixation d'une technique radionnelle," *CR Acad. Sci.*, vol. 143, pp. 983–995, 1906.

[44] H. Vanmarcke, "Stralingsbescherming deel 2: organisatie, wetgeving en risicocommunicatie," 2018.

[45] H. Cember *et al.*, *Introduction to health physics*. Pergamon Press Ltd., 1969.

[46] E. J. Calabrese and L. A. Baldwin, "Hormesis: the dose-response revolution," *Annual review of pharmacology and toxicology*, vol. 43, no. 1, pp. 175–197, 2003.

[47] K. Seong, "Is the linear no-threshold dose-response paradigm still necessary for the assessment of health effects of low dose radiation?," *J Korean Med Sci*, vol. 31, 2016.

[48] ICRP, "The 2007 recommendations of the international commission on radiological protection. icrp publication 103.," *Ann ICRP*, vol. 37, no. 2.4, p. 2, 2007.

[49] A. Granov, L. Tiutin, and T. Schwarz, *Positron emission tomography*. Springer Science & Business Media, 2013.

[50] H. O. Anger, "Scintillation camera," *Review of scientific instruments*, vol. 29, no. 1, pp. 27–33, 1958.

[51] M. M. Khalil, J. L. Tremoleda, T. B. Bayomy, and W. Gsell, "Molecular spect imaging: an overview," *International journal of molecular imaging*, vol. 2011, 2011.

[52] B. J. McParland, *Nuclear medicine radiation dosimetry: advanced theoretical principles*. Springer Science & Business Media, 2010.

[53] Y.-S. Kim and M. W. Brechbiel, "An overview of targeted alpha therapy," *Tumor Biology*, vol. 33, pp. 573–590, Jun 2012.

[54] S. S. Kelkar and T. M. Reineke, "Theranostics: combining imaging and therapy," *Bioconjugate chemistry*, vol. 22, no. 10, pp. 1879–1903, 2011.

[55] C. Müller, K. Zhernosekov, U. Köster, K. Johnston, H. Dorrer, A. Hohn, N. T. van der Walt, A. Türler, and R. Schibli, "A unique matched quadruplet of terbium radioisotopes for pet and spect and for α-and β–radionuclide therapy: An in vivo proof-of-concept study with a new receptor-targeted folate derivative," *Journal of nuclear medicine*, vol. 53, no. 12, pp. 1951–1959, 2012.

[56] http://www.unscear.org/unscear/en/about_us/mandate.html. Accessed: 02-03-2019.

[57] http://www.icrp.org/page.asp?id=9. Accessed: 04-03-2019.

[58] R. Clarke and J. Valentin, "The history of icrp and the evolution of its policies: Invited by the commission in october 2008," *Annals of the ICRP*, vol. 39, no. 1, pp. 75–110, 2009.

[59] https://www.iaea.org/about/overview/history. Accessed: 04-03-2019.

[60] D. A. Howlett, *EURATOM and nuclear safeguards*. Springer, 1990.

[61] https://icru.org/icru-at-a-glance-pdf/uncategorised/icru-at-a-glance. Accessed: 05-03-2019.

[62] ICRP, "The 2009 recommendations of the international commission on radiological protection. icrp publication 109.," *Ann ICRP*, vol. 39, no. 1, pp. 1–110, 2009.

[63] ICRP, "International recommendations for x-ray and radium protection," *Ann ICRP*, 1928.

[64] ICRP, "Recommendations of the icrp. icrp publication 26," *Ann ICRP*, 1977.

[65] E. S. of Radiology, "Summary of the european directive 2013/59/euratom: essentials for health professionals in radiology," *Insights into imaging*, vol. 6, no. 4, pp. 411–417, 2015.

[66] https://fanc.fgov.be/nl/system/files/informatiedossier_vervoer_radioactieve_stoffen.pdf. Accessed: 11-03-2019.

[67] IAEA, "Regulations for the safe transport of radioactive material - 2018 edition," *Specific Safety Requirements*, no. SSR-6, 2018.

[68] https://www.wnti.co.uk/media/38413/FS2_EN_MAR13_V2.pdf. Accessed: 11-03-2019.

[69] IAEA, "Regulations for the safe transport of radioactive material," *Safety Requirements*, no. TS-R-1, 2005.

[70] IAEA, "Advisory material for the iaea regulations for the safe transport of radioactive material (2012 edition)," *Specific Safety Guide*, no. SSG-26, 2012.

[71] H. Macdonald and E. Goldfinch, "An alternative approach to the a1/a2 system for determining package contents limits and permitted releases of radioactivity from transport packages," *Packaging and Transportation of Radioactive Materials, PATRAM*, pp. 48–56, 1980.

[72] ICRP, "Nuclear decay data for dosimetric calculations. icrp publication 107.," *Ann ICRP*, vol. 38, 2008.

[73] W. Cross, N. Freedman, J. Mainville, *et al.*, "Tables of beta-ray dose distributions in water, air and other media," tech. rep., Atomic Energy of Canada Ltd., 1982.

[74] ICRP, "Human respiratory tract model for radiological protection. icrp publication 66," *Ann ICRP*, vol. 24, pp. 1–3, 1994.

[75] ICRP, "Dose coefficients for intakes of radionuclides by workers. icrp publication 68," *Ann ICRP*, vol. 24, 1994.

[76] I. A. E. A. Food and A. O. of the United Nations. International Labour Organisation. OECD Nuclear Energy Agency. World Health Organization. Pan American Health Organization, *International Basic Safety Standards for Protection Against Ionizing Radiation and for the Safety of Radiation Sources.(Interim Ed).* International Atomic Energy Agency, 1994.

[77] W. Cross, N. Freedman, and P. Wong, "Beta ray dose distributions from skin contamination," *Radiation protection dosimetry*, vol. 40, no. 3, pp. 149–168, 1992.

[78] S. Benassai, "Bologna l re-evaluation of qa and qb values on the basis of complete spectra for gamma, x and beta emissions.(1994). rome," tech. rep., ANPA-DIR/NOR-RT-2 (94), 1994.

[79] ICRP, "Data for use in protection against external radiation. icrp publication 51," *Ann ICRP*, vol. 17, 1987.

[80] J. Hubbell, "Photon mass attenuation and energy-absorption coefficients," *The International Journal of Applied Radiation and Isotopes*, vol. 33, no. 11, pp. 1269–1290, 1982.

[81] W. Cross, N. Freedman, and P. Wong, "Beta-ray dose distributions from point sources in an infinite water medium.," *Health physics*, vol. 63, no. 2, pp. 160–171, 1992.

[82] M. J. Berger and S. M. Seltzer, "Stopping powers and ranges of electrons and positions," tech. rep., NATIONAL STANDARD REFERENCE DATA SYSTEM, 1982.

[83] K. Jones, T. Cabianca, M. Harvey, J. Hughes, I. Brown, and T. Anderson, *Review of Methodologies to Calculate A1 and A2 Values, and Exemption Values.* Health Protection Agency, 2011.

[84] D. Castelianos and W. E. Rosenthal, "Rational chebyshev approximations of analytic functions," *The Fibonacci Quarterly*, vol. 31, no. 3, pp. 205–215, 1993.

[85] P. J. Davis, *Interpolation and approximation.* Courier Corporation, 1975.

[86] H. Verhoeven, "Tb radioisotopes for medical applications," Master's thesis, KU Leuven, Belgium, 2018.

[87] A. Burgoyne, M. Ooms, D. Elema, and T. Cardinaels, "Tb-161 purification by high performance ion chromatography (hpic) from irradiated gd-160," *Journal of Labelled Compounds and Radiopharmaceuticals*, no. 62, 2019.

[88] K. Jones, M. Harvey, S. Hughes, I. Brown, and T. Anderson, "Review of the methodologies and development of software to calculate exemption and a1 and a2 values," tech. rep., Health Protection Agency, 09 2009.

[89] K. Kawai, H. Noguchi, and A. Endo, "Dose coefficients for radionuclides produced in high energy proton accelerator facilities. coefficients for radionuclides not listed in icrp publications," tech. rep., JAERI-DATA-CODE-2002-013, 2002.

[90] T. Böhlen, F. Cerutti, M. Chin, A. Fassò, A. Ferrari, P. Ortega, A. Mairani, P. R. Sala, G. Smirnov, and V. Vlachoudis, "The fluka code: developments and challenges for high energy and medical applications," *Nuclear data sheets*, vol. 120, pp. 211–214, 2014.

[91] A. Fasso, A. Ferrari, J. Ranft, and P. R. Sala, "Fluka: a multi-particle transport code," tech. rep., CERN-2005-10, 2005.

[92] V. Vlachoudis, "Flair for fluka," tech. rep., CERN, 2006.

[93] M. Pelliccioni, "Overview of fluence-to-effective dose and fluence-to-ambient dose equivalent conversion coefficients for high energy radiation calculated using the fluka code," *Radiation Protection Dosimetry*, vol. 88, no. 4, pp. 279–297, 2000.

[94] P. Bertreix and T. Frosio, "Determination of quantities of radiological interest for the shipping of radioactive goods," tech. rep., IRPA, 2018.

DEPARTEMENT NATUURKUNDE EN STERRENKUNDE
Celestijnenlaan 200d bus 2412
3001 Heverlee, BELGIË
tel. + 32 16 32 71 24
fys.kuleuven.be